

Covalency in Highly Polar Bonds. Structure and Bonding of Methylalkalimetal Oligomers (CH₃M)_n (M = Li–Rb; n = 1, 4)

F. Matthias Bickelhaupt,^{*,†} Miquel Solà,^{*,‡} and Célia Fonseca Guerra[†]

Afdeling Theoretische Chemie, Scheikundig Laboratorium der Vrije Universiteit, De Boelelaan 1083, NL-1081 HV Amsterdam, The Netherlands, and Institut de Química Computacional, Universitat de Girona, Campus Montilivi, E-17071 Girona, Catalonia, Spain

Received December 28, 2005

Abstract: We have carried out a theoretical investigation of the methylalkalimetal monomers CH₃M and tetramers (CH₃M)₄ with M = Li, Na, K, and Rb and, for comparison, the methyl halides CH₃X with X = F, Cl, Br, and I, using density functional theory (DFT) at BP86/TZ2P. Our purpose is to determine how the structure and thermochemistry (e.g., C–M bond lengths and strengths, oligomerization energies) of organoalkalimetal compounds depend on the metal atom and to understand the emerging trends in terms of quantitative Kohn–Sham molecular orbital (KS-MO) theory. The C–M bond becomes longer and weaker, both in the monomers and tetramers, if one descends the periodic table from Li to Rb. Quantitative bonding analysis shows that this trend is not only determined by decreasing electrostatic attraction but also, even to a larger extent, by the weakening in orbital interactions. The latter become less stabilizing along Li–Rb because the bond overlap between the singly occupied molecular orbitals (SOMOs) of CH₃[•] and M[•] radicals decreases as the metal ns atomic orbital (AO) becomes larger and more diffuse. Thus, the C–M bond behaves as a typical electron-pair bond between the methyl radical and alkalimetal atom, and, in that respect, it is covalent. It is also shown that such an electron-pair bond can still be highly polar, in agreement with the large dipole moment. Interestingly, the C–M bond becomes less polar in the methylalkalimetal tetramers because metal–metal interactions stabilize the alkalimetal orbitals and, in that way, make the alkalimetal effectively less electropositive.

1. Introduction

Organoalkalimetal compounds, in particular organolithium reagents, are widely used in synthetic organic and organometallic chemistry.¹ Their methyl derivatives constitute the simplest organometallic compounds and contain the archetypal carbon–metal bond. Numerous theoretical^{2–5} and experimental^{6–8} studies have been undertaken to obtain

information about structure, stability, and bonding of this class of systems. Recently, Grotjahn and co-workers^{6a–c} published the first highly accurate gas-phase experimental structures for monomeric methyllithium, -sodium, and -potassium. These species have C_{3v} symmetry and consist of a pyramidal methyl group bound to the metal atom (Chart 1, left). The C–M bond distance increases along this series, as one might expect, from 1.961 to 2.299 to 2.633 Å (Table 1).

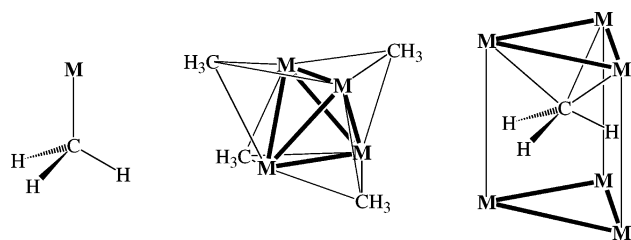
In the condensed phase, organoalkalimetal systems tend to oligomerize. Weiss and co-workers^{7a–d} have determined the crystal structure of deuterated methyllithium, -sodium,

* Corresponding author fax: +31 - 20 - 59 87 629; e-mail: FM.Bickelhaupt@few.vu.nl (F.M.B.) and fax: +34 - 972 - 41 83 56; e-mail: miquel.sola@udg.es (M.S.).

[†] Scheikundig Laboratorium der Vrije Universiteit.

[‡] Universitat de Girona.

Chart 1



and -potassium oligomers. Descending the periodic table, the C–M bond again elongates, but it is systematically longer, by up to ca. 0.4 Å, than in the corresponding monomers (Table 1). The crystal structure of methyl lithium is composed of tetramers with T_d symmetry in which a central, tetrahedral lithium cluster is surrounded by four pyramidal methyl groups, one on each face of the metal tetrahedron, in a staggered orientation with respect to the adjacent Li_3 group (Chart 1, center). The methylsodium crystal has a somewhat more involved structure with a $(\text{CD}_3\text{Na})_{16}$ unit cell that, however, still consists 50% of tetramers similar to those of methyl lithium but slightly distorted. The methylpotassium crystal, on the other hand, has a $(\text{CD}_3\text{K})_6$ unit cell in which pyramidal methyl groups are located within a trigonal prism of potassium atoms and point with the vacant site of the sp^3 -carbon atom toward one of the K_3 faces (Chart 1, right).

Many studies have been directed toward unraveling the nature of the bonding in organoalkalimetal oligomers. The current picture^{2–4f} of the carbon–lithium bond is that of an ionic bond which can best be understood in terms of a CH_3^- anion and an Li^+ cation interacting predominantly electrostatically with only marginal covalent character. Streitwieser and co-workers² were the first to emphasize the highly polar character of this bond, based on atomic charges computed with the integrated projected populations (IPP) scheme. This approach yields an atomic charge of Li in methyl lithium of +0.8 au. Also other studies have been in support of a lithium atomic charge close to +1 au, for example, natural population analysis (NPA)^{3d,5} and atoms in molecules (AIM),^{4f,i} which yield charges close to +0.9 au. In addition, Streitwieser, Bushby, and Steel have shown that a simple electrostatic model is able to reproduce the ratio of carbon–carbon and lithium–lithium distances in the methyl lithium tetramer.^{3j,k} These results have led to the current idea that the C–Li bond is 80–90% ionic.

There are also data supporting a more prominent role of covalency in the C–Li bond. Early pioneering studies by the groups of Schleyer and Pople,^{4h} Lipscomb,⁴ⁱ and Ahlrichs^{4g} have highlighted these covalent aspects, especially in organolithium aggregates. This view is experimentally supported by the large carbon–lithium NMR coupling constants of up to 17 Hz that have been measured for organolithium aggregates^{8a–d} and by the solubility of simple organolithium compounds in nonpolar solvents.^{8e,f} Also, Streitwieser's aforementioned ideal distance ratio is not found for $(\text{LiH})_4$, $(\text{LiOH})_4$, and $(\text{LiF})_4$, and for the two latter, a simple electrostatic model erroneously predicts a planar eight-membered ring to be more stable than a tetrahedral structure.^{4j} Moreover, it has been pointed out that atomic charges are no absolute quantities and can, therefore, not serve as

absolute bond-polarity indicators.⁹ Different atomic-charge schemes yield different absolute values for one and the same atom in exactly the same chemical environment. For example, while the AIM atomic charge of +0.9 au for Li in methyl lithium suggests a nearly complete transfer of one electron, GAPT, Hirshfeld, and VDD sketch a far more moderate picture with lithium atomic charges of only +0.4, +0.5, and +0.4 au, respectively.^{4k,5,9} This undermines the main argument in support of an ionic C–Li bonding mechanism.

In the present study, we have undertaken a detailed investigation of methylalkalimetal monomers CH_3M and tetramers $(\text{CH}_3\text{M})_4$, with $\text{M} = \text{Li}, \text{Na}, \text{K},$ and Rb , using the generalized gradient approximation (GGA) of density functional theory (DFT) at the BP86/TZ2P level.¹⁰ We aim at three objectives. First, we wish to obtain a set of consistent structural and thermochemical data for methylalkalimetal monomers and tetramers (geometries, C–M bond strengths, tetramerization energies); all obtained at the same level of theory. This complements the available experimental and theoretical data, which are scarce for the monomers and missing for the oligomers of the heavier methylalkalimetal systems (beyond lithium), and it enables a systematic analysis of trends.

Second, our main purpose is to better understand the physics and the nature of the carbon–alkalimetal bond based on quantitative molecular orbital (MO) theory as contained in Kohn–Sham density functional theory.¹⁰ In particular, we wish to obtain a bonding *mechanism*, that is, an understanding of how the MO electronic structures of the methyl radical and metal atom interfere, how this provides C–M bonding, and how this makes the bond polar. Through a quantitative bond energy decomposition, we assess the importance of electrostatic attraction and orbital interactions for providing the C–M bond, and we reveal their role in determining trends therein along Li, Na, K, and Rb.¹⁰ Here, we anticipate that all C–M bonds have a strong intrinsic preference for homolytic over ionic dissociation. Interestingly, the weakening of the C–M bond that we find along $\text{M} = \text{Li}, \text{Na}, \text{K},$ and Rb is largely determined by the decreasing bond overlap between the SOMOs of the $\text{CH}_3^\bullet + \text{M}^\bullet$ radicals. Thus, the C–M bond behaves as a typical electron-pair bond between the methyl radical and alkalimetal atom, and, in that respect, it is covalent. We also show that such an electron-pair bond can still be highly polar, in agreement with the large dipole moment. Virtually covalent C–M electron-pair bonding occurs if the metal forms clusters, in our case, tetramers.

Third, we discuss various descriptors (atomic charge, wave function, energy decomposition) of covalency and ionicity, how these concepts and their descriptors can be interpreted, and to what extent they really provide information about the *mechanism* of highly polar (or less polar or nonpolar) bonds. Furthermore, we discuss homolytic ($\text{CH}_3^\bullet + \text{M}^\bullet$) versus ionic ($\text{CH}_3^- + \text{M}^+$) dissociation, and we compare carbon–metal with carbon–halogen bonds.

2. Theoretical Methods

2.1. General Procedure. All calculations were performed using the Amsterdam Density Functional (ADF) program.¹¹

Table 1. Structures (in Å, deg) of Methyl Alkalimetal Monomers and Tetramers^k

system	method	C–M	C–H	∠HCH	M–M	C–C	ref
CH ₃ Li	BP86/TZ2P	2.010	1.105	106.48			this work
	exp: mm-wave, gas phase ^a	1.961(5)	1.122(5)	107.2(1)			6a
	exp: mm-wave, gas phase ^b	1.959	1.111	106.2			6c
	exp: IR, argon matrix	2.10	1.12	107.3–109.5 ^c			6d
	HF/6-31G*	2.0013	1.0934	106.2			4f
	MP2/6-31+G*	2.005	1.099	107.3			5
	MP2/6-311G*	1.983	1.098	106.2			3e
	MP2/6-31++G**	2.004	<i>d</i>	<i>d</i>			3a
	MP2/TZ+spd	1.984	1.092	106.4			4e
	MP2/6-311+G(3df,2pd)	1.971	1.094	106.27			4c
	CASSCF(10/13)/cc-pVTZ	1.998	1.111	105.7			3h
	CCSD(T)/6-311+G(3df,2pd)	1.969	1.099	106.01			4c
	CCSD(T)/cc-pV(5,Q)Z	1.9799	1.0987	105.88			4b
CCSD(T)/MT(ae)	1.9619	1.0960	105.86			4b	
B3LYP/6-31+G*	1.986	<i>d</i>	106.4			4a	
(CH ₃ Li) ₄ ecl	BP86/TZ2P	2.199	1.111	102.23	2.418	3.579	this work
	MP2/6-31+G*	2.188	1.107	102.9	2.363	3.582	5
	HF/3-21G	2.236	1.102	103.9	2.420	3.657	3e
	B3LYP/6-31+G*	2.195	<i>d</i>	102.3	2.400	3.579	4a
(CH ₃ Li) ₄ stag	BP86/TZ2P	2.213	1.110	103.02	2.408	3.614	this work
	exp: neutron diffraction, 1.5 K ^e	2.256(6)	1.072(2)	108.2(2)	2.591(9)	3.621(6)	7a
	exp: neutron diffraction, 290 K ^e	2.209(14)	0.993(7)	110.7(6)	2.605(19)	3.511(10)	7a
	exp: X-ray, powder crystal, 290 K	2.31(5)	0.96(5)	111(8)	2.68(5)	3.68(5)	7e
	HF/3-21G	2.240	<i>d</i>	<i>d</i>	2.415	3.668	3e
CH ₃ Na	BP86/TZ2P	2.376	1.098	109.84			this work
	exp: mm-wave, gas phase ^b	2.299	1.091 ^f	107.3			6c
	HF/6-31G*	2.3236	1.0910	107.2			4f
	MP2/6-31++G**	2.342	<i>d</i>	<i>d</i>			3a
	MP2/TZ+spd	2.315	1.089	108.5			4e
	MP2/6-311+G(3df,2pd)	2.306	1.091	108.43			4c
	CCSD(T)/6-311+G(3df,2pd)	2.310	1.095	110.73			4c
(CH ₃ Na) ₄ ecl	BP86/TZ2P	2.684	1.110	102.20	3.070	4.315	this work
	BP86/TZ2P	2.675	1.109	103.09	3.059	4.300	this work
(CH ₃ Na) ₄ stag	exp: neutron+synchrotron diff., 1.5 K ^g	2.57–2.68	1.094 ^h	106.2 ^h	2.97–3.17	<i>d</i>	7b,c
CH ₃ K	BP86/TZ2P	2.747	1.100	109.14			this work
	exp: mm-wave, gas phase ^a	2.633(5)	1.135(5)	107.0(1)			6a
	HF/DZP+	2.754	1.094	106.2			3b
	MP2/DZP+	2.743	1.097	107.7			3b
	MP2/[6-31++G**] ^j	2.694	<i>d</i>	<i>d</i>			3a
	MP2/DZ+spd	2.675	1.102	106.7			4e
	CCSD(T)/(C,H)VTZ	2.661	1.097	106.6			3i
	CCSD(T)/(C,H)VTZ	2.661	1.097	106.6			3i
(CH ₃ K) ₄ ecl	BP86/TZ2P	3.000	1.112	101.47	3.724	4.658	this work
(CH ₃ K) ₄ stag	BP86/TZ2P	2.962	1.111	102.39	3.714	4.575	this work
	exp: neutron diffraction, 1.35 K ⁱ	2.947(2), 3.017(4)	1.082(4), 1.103(2)	104.8(2), 105.8(2)			7d
CH ₃ Rb	BP86/TZ2P	2.821	1.096	109.63			this work
	HF/DZP+	2.906	1.095	106.2			3b
	MP2/DZP+	2.897	1.097	107.9			3b
	MP2/[6-31++G**] ^j	2.855	<i>d</i>	<i>d</i>			3a
(CH ₃ Rb) ₄ ecl	BP86/TZ2P	3.118	1.112	101.41	3.906	4.817	this work
(CH ₃ Rb) ₄ stag	BP86/TZ2P	3.068	1.110	102.35	3.893	4.707	this work

^a Partial r_s structure. ^b r_0 structure. ^c Estimated value range. ^d Value not specified. ^e (CD₃Li)₄ staggered. ^f Estimated value from ref 4f. ^g Staggered (CD₃Na)₄ unit in more complex (CD₃Na)₁₆ unit cell. ^h Average of six similar values. ⁱ Basis for K and Rb: 9VE-ECP MWB 6s6p2d/5s5p2d. ^j Staggered [(CD₃)K₃] unit in more complex (CD₃K)₆ unit cell which contains no (CH₃K)₄ units! Instead, each methyl group is located in the center of a trigonal prism of six K atoms. C–K distances in this table correspond to close contacts, i.e., distances between C and the three K atoms of the trigonal prism toward which the lone pair of the methyl group is oriented. ^k See also Chart 1 and Figure S1.

The numerical integration was performed using the procedure developed by Boerrigter, te Velde, and Baerends.^{11e,f} The MOs were expanded in a large uncontracted set of Slater type orbitals (STOs) containing diffuse functions, which is of triple- ζ quality for all atoms and has been augmented with two sets of polarization functions: 3d and 4f on C, Li, Na;

4d and 4f on K, Rb; and 2p and 3d on H.^{11g} In addition, an extra set of p functions was added to the basis sets of Li (2p), Na (3p), K (4p), and Rb (5p). The 1s core shell of carbon and lithium, the 1s 2s 2p core shells of sodium and potassium, and the 1s 2s 3s 2p 3p 3d core shells of rubidium were treated by the frozen-core (FC) approximation.^{11d} An

auxiliary set of s, p, d, f, and g STOs was used to fit the molecular density and to represent the Coulomb and exchange-correlation potentials accurately in each SCF cycle.^{11h}

Energies and geometries were calculated using the generalized gradient approximation (GGA) of DFT at the BP86 level. GGA proceeds from the local density approximation (LDA) where exchange is described by Slater's $X\alpha$ potential¹¹ⁱ and correlation is treated in the Vosko-Wilk-Nusair (VWN) parametrization^{11j} which is augmented with nonlocal corrections to exchange due to Becke^{11k,l} and correlation due to Perdew^{11m} added self-consistently.¹¹ⁿ All open-shell systems were treated with the spin-unrestricted formalism. Bond enthalpies at 298.15 K and 1 atm (ΔH_{298}) were calculated from electronic bond energies (ΔE) and our frequency computations using standard statistical-mechanics relationships for an ideal gas.¹²

2.2. Bond Energy Decomposition. The overall bond energy ΔE is made up of two major components (eq 1):

$$\Delta E = \Delta E_{\text{prep}} + \Delta E_{\text{int}} \quad (1)$$

In this formula, the preparation energy ΔE_{prep} is the amount of energy required to deform the separate molecular fragments that are connected by the chemical bond from their equilibrium structure to the geometry that they acquire in the overall molecular system. The interaction energy ΔE_{int} corresponds to the actual energy change when the prepared fragments are combined to form the overall molecule. It is analyzed for our model systems in the framework of the Kohn–Sham MO model using a Morokuma-type decomposition of the bond into electrostatic interaction, exchange repulsion (or Pauli repulsion), and (attractive) orbital interactions (eq 2).^{10,13}

$$\Delta E_{\text{int}} = \Delta V_{\text{elstat}} + \Delta E_{\text{Pauli}} + \Delta E_{\text{oi}} \quad (2)$$

The term ΔV_{elstat} corresponds to the classical electrostatic interaction between the unperturbed charge distributions of the prepared (i.e. deformed) fragments and is usually attractive. The Pauli repulsion ΔE_{Pauli} comprises the destabilizing interactions between occupied orbitals. It arises as the energy change associated with going from the superposition of the unperturbed electron densities of two fragments, say CH_3^* and M^* , i.e., $\rho_{\text{CH}_3(\alpha)} + \rho_{\text{M}(\beta)}$, to the wave function $\Psi^0 = N A [\Psi_{\text{CH}_3(\alpha)} \Psi_{\text{M}(\beta)}]$, that properly obeys the Pauli principle through explicit antisymmetrization (A operator) and renormalization (N constant) of the product of fragment wave functions.¹⁰ It comprises the four-electron destabilizing interactions between occupied orbitals and is responsible for any steric repulsion. The orbital interaction ΔE_{oi} in any MO model, and therefore also in Kohn–Sham theory, accounts for electron-pair bonding, charge transfer (i.e., donor–acceptor interactions between occupied orbitals on one fragment with unoccupied orbitals of the other, including the HOMO–LUMO interactions), and polarization (empty-occupied orbital mixing on one fragment due to the presence of another fragment). In case of open-shell fragments, the bond energy analysis yields, for technical reasons, interaction energies that differ consistently in the order of a kcal/mol (too much stabilizing) from the exact BP86 result (because,

only in the bond energy analysis, the spin-polarization in the fragments is not accounted for). To facilitate a straightforward comparison, the results of the bond energy analysis were scaled to match exactly the regular BP86 bond energies.

The orbital interaction energy can be decomposed into the contributions from each irreducible representation Γ of the interacting system (eq 3) using the extended transition state (ETS) scheme developed by Ziegler and Rauk.^{13d,e}

$$\Delta E_{\text{oi}} = \sum_{\Gamma} \Delta E_{\Gamma} \quad (3)$$

The electron density distribution is analyzed using the Voronoi deformation density (VDD) method¹⁴ and the Hirshfeld scheme (see ref 15) for computing atomic charges, which are discussed in detail in ref 9.

3. Results and Discussion

3.1. Structures. Monomers. The structural results of our BP86/TZ2P computations are summarized in Table 1, Chart 1, and Figure S1 in the Supporting Information. The C–M bond distance in the C_{3v} symmetric methylalkalimetal monomers CH_3M increases descending the periodic table from 2.010 (Li) to 2.376 (Na) to 2.747 (K) to 2.821 Å (Rb). The C–H bond distance does not change much and amounts to ca. 1.10 Å throughout the series. The methyl group however becomes significantly less pyramidal if one goes from CH_3Li with an HCH angle of 106° to the heavier congeners which all have HCH angles of 109–110°.

This agrees satisfactorily with previous theoretical work^{3a,b,e,h,i,4a–c,e,f,5} and mm-wave experiments,^{6a,c} which also yield a monotonic increase of the C–M bond along CH_3Li , CH_3Na , CH_3K , and CH_3Rb (note that no experimental data are available for CH_3Rb and that the MP2 study by Schleyer and co-workers^{3a} is the only other theoretical study that treats the whole series consistently at the same level of theory). The experimental C–M bond lengths are however systematically shorter, by 2–4%, than our BP86/TZ2P and other theoretical values. A striking discrepancy between theory and experiment is that all theoretical approaches, up to the CCSD-(T) level,^{4c} show that from Li to the heavier alkalimetals the methyl group in CH_3M becomes significantly less pyramidal, whereas the mm-wave experiments yield little change in the HCH angle, which is always close to 107°.

Tetramers. All methylalkalimetal tetramers $(\text{CH}_3\text{M})_4$ have T_d symmetry and consist of a tetrahedral cluster of alkalimetal atoms surrounded by four methyl groups, one on each M_3 face, oriented with respect to the latter either eclipsed, for Li, or staggered, for Na, K, and Rb (see Figure S1). Tetramerization, i.e., going from CH_3M to $(\text{CH}_3\text{M})_4$, causes the C–M bond to elongate substantially by 0.2–0.3 Å, whereas the C–H bond distance increases only slightly by 0.01 Å (see Table 1). There is a remarkable increase in pyramidalization of the methyl groups as follows from the HCH angle, which decreases by 4° for lithium and up to 8° for the heavier alkalimetals. The C–M bond distance in the methylalkalimetal tetramers with the methyl groups eclipsed, $(\text{CH}_3\text{M})_4 \text{ecl}$, increases again monotonically from 2.199 (Li) to 2.684 (Na) to 3.000 (K) to 3.118 Å (Rb), as does the M–M bond distance in the central metal cluster. However,

Table 2. Homolytic and Heterolytic C–M Bond Strength (in kcal/mol) of Methyl Alkalimetal Monomers

monomer	method ^a	bond energies ^b			bond enthalpies ^d		ref
		ΔE_{homo}	ΔE_{hetero}	NIMAG ^c	ΔH_{homo}	ΔH_{hetero}	
CH ₃ Li	BP86/TZ2P	−44.8	−174.3	0	−44.0	−172.4	this work
	BP86/TZ2P//MP2/6-31+G*	−45.5	−174.2	0 ^e			5
	MP2/TZ+spd	−46.1		0			4e
	MP4(SDTQ)/6-311+G**	−44.18		0 ^f			3e
	scaled CPF/C	−46.4 ± 1.2					4 g
CH ₃ Na	B3LYP/6-311++G(2d,2p)//MP2/6-31++G**	−43.7 ^g					3a
	BP86/TZ2P	−31.0	−155.8	0	−30.3	−154.0	this work
	MP2/TZ+spd	−31.6		0			4e
CH ₃ K	B3LYP/6-311++G(2d,2p)//MP2/6-31++G**	−29.4 ^g					3a
	BP86/TZ2P	−26.6	−131.0	0	−26.2	−129.5	this work
	MP2/DZ+spd	−26.1		0			4e
CH ₃ Rb	B3LYP/basis C//MP2//basis B ^h	−26.0 ^g					3a
	BP86/TZ2P	−25.0	−124.6	0	−24.6	−123.1	this work
	B3LYP/basis C//MP2//basis B ^h	−23.4 ^g					3a

^a Energy and structure obtained at the same level of theory (unless stated otherwise). ^b Zero K electronic energies (unless stated otherwise). ^c Number of imaginary frequencies. ^d 298.15 K enthalpies. ^e Vibrational analysis at HF/6-31+G*. ^f Vibrational analysis at MP2/6-311G*. ^g Zero K electronic energy + Δ ZPE correction at HF (with 6-31+G* for C, H, Li, Na, and 9VE-ECP MWB 6s6p2d/5s5p2d for K, Rb). ^h Basis B: 6-31++G** for C, H; 9VE-ECP MWB 6s6p2d/5s5p2d for K, Rb. Basis C: 6-311++G(2d,2p) for C, H; 9VE-ECP MWB 6s6p2d/5s5p2d for K, Rb.

at variance with the monomers, not only the C–H bond distance of 1.11 Å but also the extent of pyramidalization of the methyl groups is practically constant with $\angle\text{HCH} = \text{ca. } 102^\circ$. These trends are similar for the methylalkalimetal tetramers with the methyl groups staggered, (CH₃M)₄ stag, in which the C–M bond is slightly longer for Li (by 0.01 Å) and somewhat shorter for Na–Rb (by 0.01–0.05 Å) than in the corresponding (CH₃M)₄ ecl. The C–H bonds are only marginally shorter (by 0.001–0.002 Å), and the methyl groups are only slightly less pyramidal ($\angle\text{HCH}$ increases by less than 1°) in (CH₃M)₄ stag compared to (CH₃M)₄ ecl.

There is, to the best of our knowledge, no other theoretical work on methylalkalimetal tetramers except for tetramethyl lithium. This prevents a comparison of structural trends found by us with other computations. However, our BP86/TZ2P geometries for (CH₃Li)₄ ecl are in excellent agreement with MP2/6-31+G*⁵ and B3LYP/6-31+G*^{4a} geometries (Table 1). The C–Li bond, for example, is 2.199, 2.188, and 2.195 Å at BP86, MP2, and B3LYP, respectively. Crystal structures of methyl lithium, -sodium, and -potassium always yield the staggered conformation of the methyl groups with respect to the M₃ face to which they are coordinated, whereas we find the eclipsed orientation (CH₃M)₄ ecl to be the lower-energy structure for M = Li (vide infra). The preference for (CH₃Li)₄ ecl over (CH₃Li)₄ stag that we find is confirmed by other theoretical studies^{3e,4a} (at HF/3-21G and B3LYP/6-31+G*), as is the elongation of the C–Li bond going from eclipsed to staggered (see HF/3-21G in Table 1). This is further evidence for intermolecular interactions and crystal packing effects being responsible for the experimentally observed staggered conformation (CH₃Li)₄ stag in methyl lithium crystals.^{7a,c} The importance of crystal environment and packing effects is also suggested by the increasing extent to which the methylalkalimetal aggregates in the crystal deviate from the tetrahedral tetramer structure along Li, Na, and K, as pointed out in the Introduction (see also Chart 1).⁷ The trend of increasing C–M bond distances that we find along M = Li–Rb agrees again well with the trend

emerging from crystal structures, which are available for Li–K (Table 1). No experimental data are available for methylrubidium aggregates. Our C–Li bond distance of 2.213 Å for (CH₃Li)₄ stag is between the 1.5 and 290 K neutron diffraction values of 2.256(6) and 2.204(14) Å found in the tetramers that constitute the methyl lithium crystal. Our C–Na distance of 2.675 Å for (CH₃Na)₄ stag is also between the range of 2.57–2.68 Å found for the slightly distorted tetramer units in the more complex (CD₃Na)₁₆ unit cell of the methyl sodium crystal using neutron and synchrotron diffraction techniques at 1.5 K.^{7c} And, finally, also our C–K distance of 2.962 Å for (CH₃K)₄ stag is nicely between the 1.35 K neutron diffraction values of 2.947 and 3.017 Å found for the CD₃K₃ entities in the (CD₃K)₆ unit cell of the methyl potassium crystal.

3.2. Thermochemistry. Monomers. The thermochemical results of our BP86/TZ2P calculations are collected in Tables 2 (monomers) and 3 (tetramers). Homolytic dissociation of the C–M bond in methylalkalimetal monomers (eq 4) is strongly favored over heterolytic or ionic dissociation (eq 5) for all methylalkalimetal monomers with heterolytic bond dissociation enthalpies (BDE = $-\Delta H$ in Table 2) being up to 5 times higher than the homolytic ones. This is because of the charge separation in the latter (eq 5), which is energetically highly unfavorable in the gas phase (vide infra).



Note that the C–M bond strength in methylalkalimetal monomers decreases if one descends group 1 in the periodic table. The bond enthalpies for both homolytic ($\Delta H_{\text{homo}} = -44.0, -30.3, -26.2$ and -24.6 kcal/mol) and heterolytic dissociation ($\Delta H_{\text{hetero}} = -172.4, -154.0, -129.5,$ and -123.1 kcal/mol) become less bonding along M = Li, Na, K, and Rb (Table 2). This finding is remarkable because it is *not* in line with the current idea of an “ionic” carbon–alkalimetal bond. We will come back to this in section 3.3.

Table 3. Tetramerization Energies and Enthalpies (in kcal/mol) of Methyl Alkalimetal Monomers

monomer	method ^a	tetramerization energies ^b		NIMAG ^c		tetramerization enthalpies ^d		ref
		$\Delta E_{\text{tetra}} \text{ ecl}^e$	$\Delta E_{\text{tetra}} \text{ stag}^f$	ecl ^e	stag ^f	$\Delta H_{\text{tetra}} \text{ ecl}^e$	$\Delta H_{\text{tetra}} \text{ stag}^f$	
CH ₃ Li	BP86/TZ2P	-125.3	-120.8	0	4	-120.3	-118.7	this work
	MP4(SDQ)/6-31+G* ^g	-131.5 ^g		0 ^g				5
	ab initio estimate ^h	-122.9 ^h	-116.0 ^h	0 ^h				3e
CH ₃ Na	BP86/TZ2P	-73.5	-73.6	i	i	-73.1	-73.5	this work
CH ₃ K	BP86/TZ2P	-82.1	-85.2	4	0	-81.4	-82.5	this work
CH ₃ Rb	BP86/TZ2P	-80.4	-85.2	i	i	-79.8	-87.1	this work

^a Energy and structure obtained at the same level of theory, unless stated otherwise. ^b Zero K electronic energies, unless stated otherwise. ^c Number of imaginary frequencies. ^d 298.15 K enthalpies. ^e Tetramer with methyl C–H bonds and metal atoms eclipsed. ^f Tetramer with methyl C–H bonds and metal atoms staggered. ^g Single-point calculation using MP2/6-31+G* geometry, with HF/6-31+G* ZPE correction. ^h Energies computed at HF/3-21G geometry. Difference between MP2/6-31G and HF/6-31G added to the HF/6-31G+6d(C) energy, with MNDO ZPE correction. ⁱ Numerical instabilities prevent accurate determination of NIMAG with ADF. Thermal energies and, thus, enthalpies are less sensitive.

There are no experimental data to which our bond enthalpies can be compared. However, the agreement with other theoretical studies is excellent (Table 2). These studies do not report bond enthalpies but zero K bond energies, and they do not cover heterolytic dissociation (eq 5). The trend of the decreasing homolytic C–M bond energy $\Delta E_{\text{hom}}^{\text{h}}$ is confirmed both at MP2 (computed for Li–K)^{4c} and UB3LYP (computed for Li–Rb),^{3a} and deviations with respect to our values are 1 kcal/mol or less.¹⁶ For the homolytic C–Li bond energy, there is also an MP4(SDTQ)/6-311+G** value (-44.18 kcal/mol) that differs only 0.6 kcal/mol from our BP86/TZ2P result (-44.8 kcal/mol).

Tetramers. Tetramerization is considerably more exothermic for methyllithium than for the heavier methylalkalimetals (see Table 3, Chart 1, and Figure S1). The tetramerization enthalpy of CH₃M is -120.3, -73.5, -82.5, and -87.1 kcal/mol along M = Li, Na, K, and Rb. The equilibrium structure of tetramethylithium has the methyl groups oriented eclipsed with respect to the Li₃ face to which they are coordinated. Enthalpically, the eclipsed structure ($\Delta H_{\text{tetra}} = -120.3$ kcal/mol) is however only slightly preferred over the staggered one ($\Delta H_{\text{tetra}} = -118.7$ kcal/mol), i.e., by 1.6 kcal/mol. Going from Li to Na, the staggered structure (CH₃Na)₄ stag ($\Delta H_{\text{tetra}} = -73.5$ kcal/mol) becomes slightly more stable than the eclipsed structure (CH₃Na)₄ ecl ($\Delta H_{\text{tetra}} = -73.1$ kcal/mol). Note, that the difference in tetramerization energy ΔE_{tetra} is practically zero. In other words, the methyl groups have hardly any barrier for rotation. Proceeding from Na via K to Rb, the enthalpic preference for the staggered structure increases from 0.4 to 1.1 to 7.3 kcal/mol.

No experimental tetramerization enthalpies are available. However, the fact that the methyl groups in crystal structures of methylalkalimetal compounds are found always (i.e., for Li, Na, and K) staggered with respect to the M₃ face to which they are coordinated (Table 1) agrees well with our finding that for Li this orientation is disfavored only very slightly (and can thus easily become the preferred structure through crystal packing effects) and favored for Na–Rb. Other theoretical studies on methylalkalimetal tetramers are only available for lithium (Table 1).^{3e,5} Our tetramerization energy ΔE_{tetra} of -125.3 kcal/mol is between the ab initio estimate of -122.9 kcal/mol by Kaufmann et al.^{3e} and the value of -131.5 obtained by Bickelhaupt et al.⁵ at MP4(SDQ)/6-

Table 4. Analysis of the Carbon–Metal Bond between CH₃^{*} and M^{*} in Methylalkalimetal Monomers^a

	CH ₃ –Li	CH ₃ –Na	CH ₃ –K	CH ₃ –Rb
Bond Energy Decomposition (in kcal/mol)				
ΔE_{A1}	-62.1	-41.7	-37.9	-41.5
ΔE_{E1}	-1.0	-0.5	-0.5	-0.7
ΔE_{O1}	-63.1	-42.2	-38.4	-42.2
ΔE_{Pauli}	38.4	27.8	23.4	30.7
ΔV_{elstat}	-30.3	-23.3	-19.0	-20.4
ΔE_{int}	-55.0	-37.7	-34.0	-31.9
ΔE_{prep}	10.2	6.7	7.4	6.9
ΔE_{hom}	-44.8	-31.0	-26.6	-25.0
Fragment Orbital Overlaps				
$\langle 1a_1 ns \rangle^b$	0.32	0.27	0.24	0.23
$\langle 2a_1 ns \rangle^b$	0.31	0.28	0.21	0.19
$\langle 1e_1 np_{\pi} \rangle^b$	0.22	0.18	0.14	0.14
Fragment Orbital Interaction Matrix Elements (in kcal/mol)				
$\langle 2a_1 F ns \rangle^b, c$	-42.2	-39.1	-25.3	c
Fragment Orbital Populations (in electrons)				
CH ₃				
1a ₁	1.95	1.99	2.00	2.01
2a ₁	1.40	1.42	1.48	1.45
1e ₁	1.96	1.96	1.97	1.96
M				
ns ^b	0.50	0.56	0.46	0.49
np _o ^b	0.18	0.03	0.02	0.03
np _π ^b	0.03	0.01	0.01	0.01

^a At BP86/TZ2P. See section 2.2 for explanation of energy terms. ^b n = 2, 3, 4 and 5 for M = Li, Na, K, and Rb, respectively. ^c Computed with the fully converged SCF density of CH₃M. Cannot yet be computed for Rb, for technical reasons.

31+G*. The former study^{3e} also confirms the energetic preference for the structure with eclipsed over that with staggered methyl groups (in the latter, this has not been investigated).

3.3. Analysis of the C–M Bond in CH₃M Monomers.

The analyses of the electronic structure and bonding mechanism in methylalkalimetal monomers CH₃M reveal both substantial covalent character for the C–M bond (see Table 4 and Figures 1–3) and a high polarity (see also the section on “Heterolytic Dissociation”, below). In the first place, for all four alkalimetals, the C–M bond is characterized by substantial mixing between the methyl 2a₁ SOMO and the alkalimetal ns AO in the 2a₁ + ns electron-pair bonding

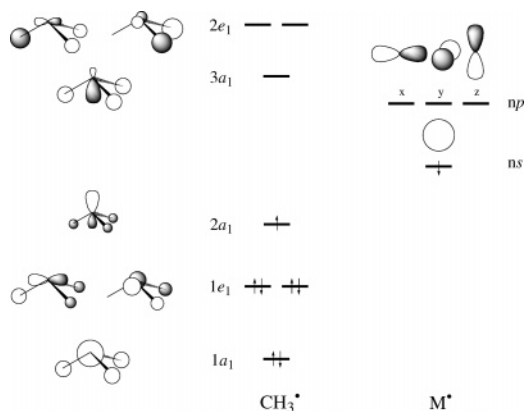


Figure 1. Schematic representation of the valence orbitals of CH_3^* and M^* ($n = 2, 3, 4,$ and 5 for $\text{M} = \text{Li}, \text{Na}, \text{K},$ and Rb).

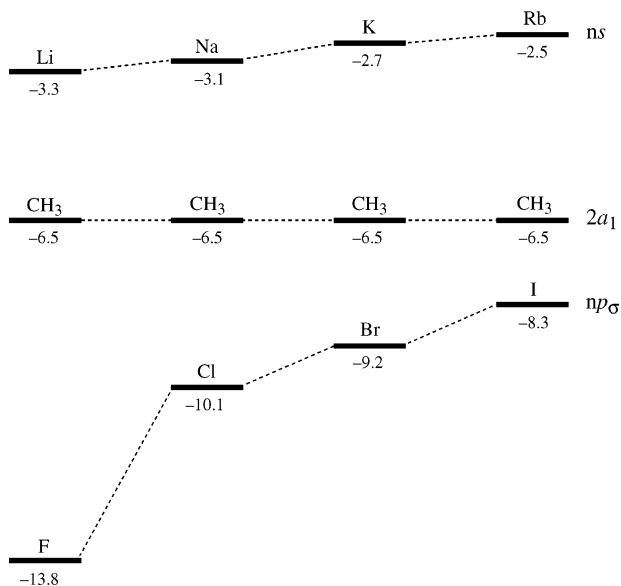


Figure 2. Energies (in eV) of the SOMOs of CH_3^* (in the geometry it adapts in CH_3Li), alkali metal atoms M^* , and halogen atoms X^* at BP86/TZ2P.

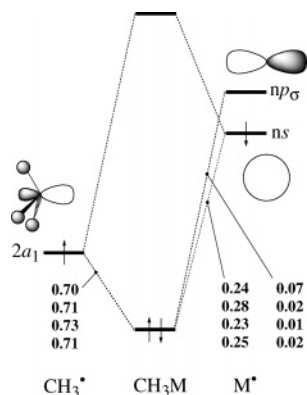


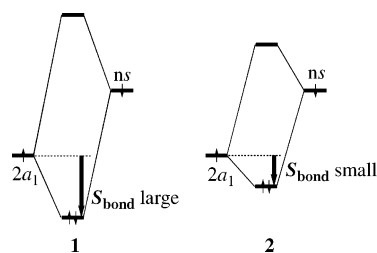
Figure 3. Orbital interaction diagram for CH_3M with Gross Mulliken contributions at BP86/TZ2P of CH_3^* and M^* fragment orbitals to the C–M electron-pair bonding MO for $\text{M} = \text{Li}, \text{Na}, \text{K},$ and Rb .

combination (see Figures 1 and 3). While it is true that the electron-pair bonding $2a_1 + ns$ combination is polarized toward methyl, the alkali metal ns contribution is significant and not at all marginal: in terms of Gross Mulliken

contributions¹⁷ the composition is approximately 70% $2a_1 + 25\%$ ns (see Figure 3). In case of methyl lithium, the situation is 70% $2a_1 + 24\%$ $2s$ with, in addition, a sizable contribution of 7% from the lithium $2p_\sigma$ AO. In terms of mixing coefficients, this is $0.72 2a_1 + 0.53 2s (+ 0.32 2p_\sigma)$.

The above mixing is indicative for substantial $2a_1 + ns$ orbital interaction, which is confirmed by further analyses. Indeed, the bond interaction-matrix elements $F_{\text{bond}} = \langle 2a_1 | F | ns \rangle$ between the two SOMOs are strongly stabilizing with values ranging from -42.2 (Li) via -39.1 (Na) to -25.3 kcal/mol (K) (see Table 4; F is the effective one-electron Hamiltonian or Fock operator evaluated with the fully converged SCF density of the molecule). We recall that the stabilization $\Delta\epsilon$ of our electron-pair bonding $2a_1 + ns$ combination with respect to $\epsilon(2a_1)$ is, in second order (and neglecting the effect of other occupied and virtual orbitals!), given by $\langle 2a_1 | F | ns \rangle^2 / \epsilon(2a_1) - \epsilon(ns)$, that is, the interaction-matrix element squared divided by the difference in orbital energies.¹⁸ Thus, according to this approximate relationship, the stabilization $\Delta\epsilon$ is a sizable 24 kcal/mol for the C–Li bond, 19 kcal/mol for the C–Na bond, and 7 kcal/mol for the C–K bond (see $\epsilon(2a_1)$, $\epsilon(ns)$, and $\langle 2a_1 | F | ns \rangle$ values in Figure 2 and Table 4). This is a weakening along the C–Li, C–Na, and C–K bonds.

This trend can be straightforwardly understood in terms of the corresponding bond overlap $S_{\text{bond}} = \langle 2a_1 | ns \rangle$, which is sizable and decreases from 0.31 to 0.28 to 0.21 to 0.19 along $\text{M} = \text{Li}, \text{Na}, \text{K},$ and Rb (Table 4). This is caused by the metal ns AOs becoming more diffuse and extended along this series, leading to smaller optimum overlap at longer bond distance.¹⁹ This mechanism, which causes the C–M bond to weaken along Li, Na, K as observed, is illustrated by 1 and 2, below:



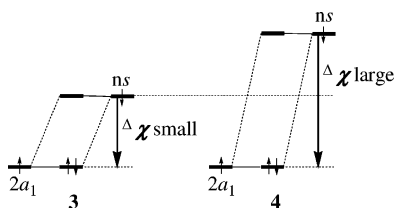
These illustrations show how the stabilization of the electrons in the bonding $2a_1 + ns$ combination is reduced if one goes from a situation with stronger (1) to a situation with weaker (2) $\langle 2a_1 | ns \rangle$ overlap and orbital interaction.

The above picture is confirmed by our quantitative bond energy decomposition. The exact (within our Kohn–Sham MO approach) values of the orbital interactions ΔE_{oi} are clearly larger than the above estimates. Importantly, they are of decisive importance and they show again the same trend. Along the C–Li, C–Na, and C–K bonds, the orbital interactions ΔE_{oi} weaken from -63.1 to -42.2 to -38.4 kcal/mol. The trend resulting from the orbital interactions is further enhanced by the electrostatic attraction ΔV_{elstat} . The latter also weakens along this series owing to the decreasing overlap between occupied orbitals of CH_3^* and M^* because the metal AOs become more extended and diffuse and the C–M bond length increases. For the same reason, the Pauli

repulsion becomes less repulsive along Li, Na, and K. Note that the dominant contributor to the trend in the overall C–M bond energy ΔE is the orbital interactions ΔE_{oi} . Thus, the trend in the thermodynamic stability ΔE (or $\Delta H^{298} = -\text{BDE}$) of the C–M bond, i.e., the weakening along Li, Na, and K, can be related directly to covalent features in the bonding mechanism: the bond overlap between and mixing of the SOMOs that yield the electron-pair bond.

From K to Rb the trend is determined by a more involved and subtle interplay of factors, and we restrict ourselves to the main effect. The step from K to Rb involves the introduction of the first subvalence d shell, i.e., $3d$. This has relatively little effect on the spatial extent of the ns AO, which expands slightly. The bond overlap $\langle 2a_1 | ns \rangle$ further decreases from K to Rb but more slightly so than before (from Na to K). Note however that the $2a_1 + ns$ mixing in CH_3Rb remains substantial (see Figure 3). In the end, the effect of the slight reduction in bond overlap is delicately overruled by that of the increase in stabilization of the electron stemming from the metal ns AO as the orbital energy $\epsilon(ns)$ rises from -2.7 (K) to -2.5 eV (Rb): the orbital interaction ΔE_{oi} becomes somewhat more stabilizing (Table 4 and Figure 2). The presence of the 10 electrons in the subvalence $3d$ shell has a more pronounced effect on the Pauli repulsion: going from K to Rb it becomes 7 kcal/mol more repulsive. This is the reason why overall the C–M bond strength continues to decrease.

Finally, it is interesting to note that if the ionic picture^{2–4f} were correct, one would obtain a trend in orbital interactions that is opposite to the actually observed one. If the C–M bond were predominantly ionic with marginal covalent contributions, the MO carrying the bonding electron pair would have only a slight contribution of the metal ns AO. In other words, this MO would resemble the methyl anion $2a_1$ lone-pair orbital rather than a bonding $2a_1 + ns$ combination. Consequently, it would be hardly stabilized with respect to the methyl $2a_1$ fragment MO. This ionic bonding mechanism is schematically shown in **3** ($\Delta\chi$ refers to the electronegativity difference defined in terms of the orbital-energy difference $\epsilon(2a_1) - \epsilon(ns)$, see ref 20):



In this (fictitious) ionic picture, the electron simply drops from the metal ns into the methyl $2a_1$ giving rise to a stabilization that equals the orbital energy difference $\epsilon(2a_1) - \epsilon(ns)$, indicated in **3** by a bold arrow. Thus, one would expect that the C–M orbital interaction ΔE_{oi} increases if the metal AO energy $\epsilon(ns)$ rises, that is, if the alkalimetal becomes more electropositive, because, as shown in **4**, the electron originating from the metal would experience a larger stabilization energy $\epsilon(2a_1) - \epsilon(ns)$. But, above, we have already seen that the opposite happens: the C–M orbital interaction ΔE_{oi} decreases (Table 4: $\Delta E_{oi} = -63.1, -42.2,$

Table 5. Analysis of the Carbon–Metal Bond between $(\text{CH}_3)_4$ and $(\text{M})_4$ in Methyl Alkalimetal Tetramers^a

	$(\text{CH}_3\text{-Li})_4^b$	$(\text{CH}_3\text{-Na})_4^b$	$(\text{CH}_3\text{-K})_4^c$	$(\text{CH}_3\text{-Rb})_4^c$
Bond Energy Decomposition (in kcal/mol)				
ΔE_{A1}	-84.0	-58.5	-63.3	-62.4
ΔE_{T2}	-388.1	-269.0	-265.5	-271.6
ΔE_{rest}	-18.0	-4.5	-4.7	-5.0
ΔE_{oi}	-490.1	-332.0	-333.5	-339.0
ΔE_{Pauli}	502.2	243.4	254.7	268.1
ΔV_{elstat}	-377.8	-190.1	-187.0	-194.6
ΔE_{int}	-365.7	-278.7	-265.8	-265.5
$\Delta E_{\text{prep}}[\text{M}_4]^d$	-6.7	16.4	10.7	16.9
$\Delta E_{\text{prep}}[(\text{CH}_3)_4]^d$	67.9	64.8	63.5	63.4
ΔE_{homo}^d	-304.5	-197.5	-191.6	-185.2
Fragment Orbital Overlaps				
$\langle (\text{CH}_3)_4 (\text{M})_4 \rangle$				
$\langle 2a_1 qa_1 \rangle^e$	0.55	0.49	0.39	0.35
$\langle 3t_2 rt_2 \rangle^f$	0.28	0.24	0.18	0.17
$\langle \text{CH}_3 \text{CH}_3 \rangle$				
$\langle 2a_1 2a_1 \rangle$	0.08	0.04	0.03	0.02
$\langle \text{M} \text{M} \rangle$				
$\langle ns ns \rangle^g$	0.63	0.52	0.49	0.49
$\langle ns np_o \rangle^g$	0.41	0.40	0.40	0.33
Fragment Orbital Populations (in electrons)				
$(\text{CH}_3)_4$				
$2a_1$	1.07	1.29	1.55	1.58
$3t_2$	1.48	1.66	1.65	1.55
$(\text{M})_4$				
qa_1^e	0.84	0.67	0.26	0.26
rt_2^f	0.57	0.21	0.12	0.15

^a At BP86/TZ2P. ^b Tetramer with methyl C–H bonds and metal atoms eclipsed. ^c Tetramer with methyl C–H bonds and metal atoms staggered. ^d $\Delta E_{\text{prep}}[(\text{CH}_3)_4] = \Delta E_{\text{prep}}[4\text{CH}_3^* \rightarrow (\text{CH}_3)_4]$, $\Delta E_{\text{prep}}[\text{M}_4] = \Delta E_{\text{prep}}[4\text{M}^* \rightarrow \text{M}_4]$ and $\Delta E = \Delta E[4\text{CH}_3^* + 4\text{M}^* \rightarrow (\text{CH}_3\text{M})_4]$. ^e $q = 1$ (Li, Na) or 3 (K, Rb). ^f $r = 1$ (Li, Na) or 4 (K, Rb). ^g $n = 2, 3, 4, 5$ for $\text{M} = \text{Li, Na, K, and Rb}$, respectively.

–38.4 kcal/mol) as the metal becomes more electropositive (Figure 2: $\epsilon(ns) = -3.3, -3.1, -2.7$) along $\text{M} = \text{Li, Na, and K}$ (see also ref 20a).

In conclusion, the C–M bond has substantial covalent character stemming from bond overlap that determines largely the trend in bond strength descending the periodic table in group 1. The fact that part of the stabilization stems from bond overlap is not in contradiction with this bond being highly polar.

3.4. Analysis of the C–M Bond in CH_3M Tetramers.

Tetramerization further enhances the covalent character of the C–M bond, as follows from our computations (see Table 5 and Figures 4–6). The C–M bond in the methylalkalimetal tetramers has been analyzed in terms of the interaction between the outer tetrahedron of methyl groups $(\text{CH}_3)_4$ and the inner tetrahedral metal cluster M_4 . The frontier orbitals of both fragments $(\text{CH}_3)_4$ and M_4 are energetically arranged in the three-over-one pattern characteristic for tetrahedral species: the bonding combination of four methyl $2a_1$ or alkalimetal ns AOs at low orbital energy in A_1 symmetry and the corresponding three antibonding combinations at high orbital energy in T_2 symmetry (see Figure 4). In the valence state of $(\text{CH}_3)_4$ and M_4 , each of these orbitals is singly occupied, and the lowest energy for this configuration is achieved if the four unpaired electrons on either fragment

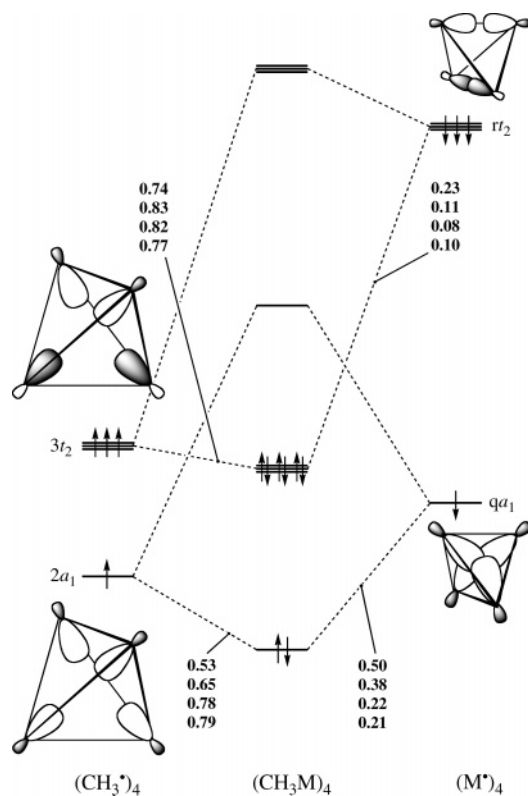


Figure 4. Orbital interaction diagram for $(\text{CH}_3\text{M})_4$ with Gross Mulliken contributions of $(\text{CH}_3^*)_4$ and $(\text{M}^*)_4$ fragment orbitals to the C–M electron-pair bonding MOs in A_1 and T_2 symmetry for $M = \text{Li, Na, K, and Rb}$. For clarity, only one of the 3-fold degenerate $3t_2$ and rt_2 orbitals of $(\text{CH}_3^*)_4$ and $(\text{M}^*)_4$, respectively, is visualized.

have equal spin. Note that this configuration leads in principle to $\text{CH}_3\text{--CH}_3$ and M--M repulsion. In the methylalkalimetal tetramer, four C–M electron-pair bonds are formed between $(\text{CH}_3)_4$ and M_4 : the $2a_1 + qa_1$ combination and the three degenerate $3t_2 + rt_2$ combinations.

Before further examining these bonds, it is important to take a closer look at the formation of the $(\text{CH}_3)_4$ and M_4 fragments from individual methyl radicals and alkalimetal atoms, respectively. The formation of the $(\text{CH}_3)_4$ tetrahedron from four methyl radicals is relatively endothermic with preparation energies $\Delta E_{\text{prep}}[(\text{CH}_3)_4]$ of 63–68 kcal/mol (see Table 5). The major part of this preparation energy, i.e., 62–63 kcal/mol (not shown in Table 5), is associated with methyl pyramidalization caused by the eventual interaction with the alkalimetal cluster in $(\text{CH}_3\text{M})_4$. The remaining part of $\Delta E_{\text{prep}}[(\text{CH}_3)_4]$, that is, the repulsion between the methyl radicals in the $(\text{CH}_3)_4$ tetrahedron is relatively small and decreases from 5.1 to 1.6 to 1.5 to 1.4 kcal/mol along $M = \text{Li, Na, K, and Rb}$ (not shown in Table 5). The reason is simply that the methyl radicals in $(\text{CH}_3)_4$ are far away from each other ($\text{C--C} = 3.597\text{--}4.707 \text{ \AA}$ along Li--Rb , see Table 1) and the methyl $2a_1$ SOMOs cannot build up much overlap ($\langle 2a_1|2a_1 \rangle = 0.08\text{--}0.02$, see Table 5). Therefore, they enter into an only weakly repulsive orbital interaction. This is also reflected by the small energy splitting between the bonding $2a_1$ and antibonding $3t_2$ orbitals of $(\text{CH}_3)_4$ shown in Figure 5.

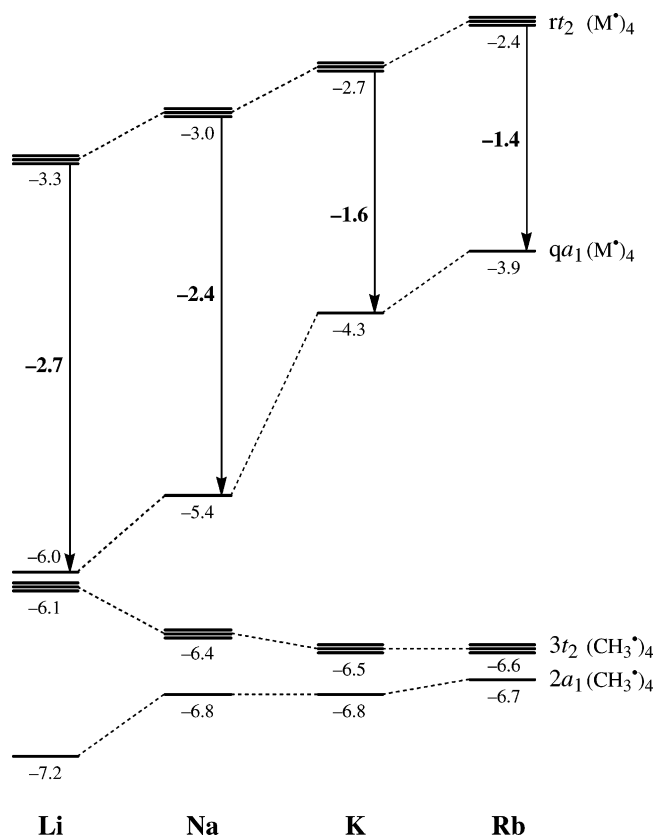


Figure 5. Energies (in eV) of the SOMOs of $(\text{CH}_3^*)_4$ and $(\text{M}^*)_4$ fragments in their valence state in the corresponding methyl alkalimetal tetramers $(\text{CH}_3\text{M})_4$ (eclipsed for Li, Na , staggered for K, Rb , see Figure S1; $q = r = 1$ for $M = \text{Li and Na}$, or $q = 3$ and $r = 4$ for $M = \text{K and Rb}$).

An interesting phenomenon occurs in the alkalimetal clusters M_4 . The metal atoms are in close contact ($\text{M--M} = 2.418\text{--}3.893 \text{ \AA}$ along Li--Rb , see Table 1) leading to remarkably large overlaps between the metal ns AOs ($\langle ns|ns \rangle = 0.63\text{--}0.49$, see Table 5). On the basis of this, one would expect a large energy splitting between the bonding qa_1 and antibonding rt_2 orbitals of the M_4 cluster and, accordingly, a strong M--M repulsion for all alkalimetals. The energy splitting between the bonding qa_1 and antibonding rt_2 combinations is indeed large, especially for Li_4 (see Figure 5). Yet, the preparation energy $\Delta E_{\text{prep}}[\text{M}_4]$ for the lithium cluster is not repulsive but stabilizing by -6.7 kcal/mol. The origin of this effect is stabilizing $ns\text{--}np$ mixing, as illustrated in Figure 6. This occurs in all four metal clusters, but the effect is particularly strong in case of lithium whose $2p$ AOs are at rather low energy. This makes the alkalimetal cluster effectively more electronegative than the isolated alkalimetal atom: the antibonding rt_2 orbitals of the M_4 cluster end up approximately at the same energy as the corresponding ns AOs (instead of at higher orbital energy), and the bonding qa_1 combinations drop enormously in energy, by 2.7, 2.4, 1.6, and 1.4 eV along Li--Rb (Figure 5).

The above has important consequences for the four C–M electron-pair bonds between $(\text{CH}_3)_4$ and M_4 in the methylalkalimetal tetramers. The qa_1 SOMO of Li_4 (at -6.0 eV) is stabilized so much that it begins to approach the energy of the $2a_1$ SOMO of $(\text{CH}_3)_4$ (at -7.2 eV) with which it forms an electron-pair bond (see Figures 4 and 5). This results in

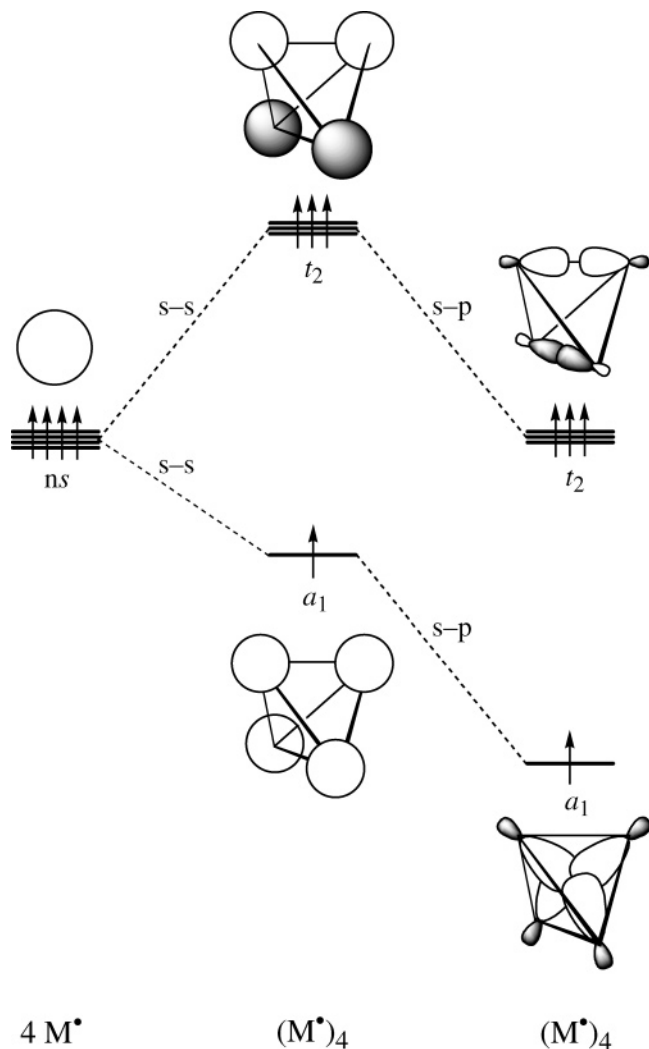


Figure 6. Formation of the SOMOs of the tetrahedral $(M^*)_4$ fragment in its valence state involves two principal interactions: (i) repulsive 4-center-4-electron interaction between the ns AOs of the four atoms (s - s mixing) and (ii) stabilizing admixture of np -derived orbitals (s - p mixing).

a virtually covalent $2a_1 + qa_1$ electron-pair bond with Gross Mulliken contributions¹⁷ of $(CH_3)_4$ (53%) and M_4 (50%) nearly in perfect balance. Thus, in this bond, there is essentially no transfer of charge from lithium to carbon. Going to the methylsodium tetramer, the $2a_1 + qa_1$ electron-pair bond becomes more polarized, but polarity is still reduced if compared to the situation in the monomer (compare Figures 3 and 4). Thereafter, if one goes to potassium and rubidium, the energy of the qa_1 SOMO of M_4 increases steeply, and the $2a_1 + qa_1$ electron-pair bond is no longer less polar in the tetramer than in the monomer. Note that the trend in the corresponding orbital interaction term ΔE_{A1} is dominated by the bond overlap $\langle 2a_1 | qa_1 \rangle$, which decreases from 0.55 to 0.35 along Li–Rb, except for the step from Na to K for which the qa_1 orbital energy leaps from -5.4 to -4.3 eV causing a bond polarization-driven strengthening of ΔE_{A1} as illustrated by **3** and **4** (see Table 5 and Figures 4 and 5). On the other hand, the three degenerate $3t_2 + rt_2$ combinations are, for all four alkali metals, polarized

74–83% toward the methyl tetrahedron, similar to but somewhat more polar than the $2a_1 + ns$ electron-pair bonding combination in the corresponding methylalkalimetal monomers (70–73%, Figure 3). Accordingly, the corresponding C–M orbital interaction energy ΔE_{T2} in the tetramer (see Table 5) is larger than but shows the same trend as ΔE_{oi} in the monomer (see Table 4): there is a pronounced weakening from Li to Na followed by a more subtle decrease from Na to K and increase from K to Rb. The combined orbital interactions ΔE_{oi} between $(CH_3)_4$ and M_4 drop markedly from Li to Na, following the trend in bond overlaps, and they increase marginally along Na–Rb, as a result of a more subtle interplay between the trend in bond overlap and orbital-energy (or electronegativity) difference. Basically, the same picture emerges for the net interaction ΔE_{int} : a strong weakening from Li to Na and marginal changes along Na, K, and Rb. The increased covalency is also found for the C–Li electron-pair bond between one single CH_3 and the Li_4 cluster in CH_3 – Li_4 (see Supporting Information).

In conclusion, the covalent character of the C–M bond increases substantially on tetramerization, especially for Li and to a lesser extent Na, because metal–metal interactions in the central M_4 cluster stabilize the alkali metal orbitals and, in that way, make the alkali metal effectively less electro-positive.

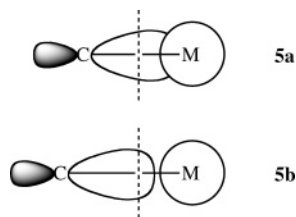
3.5. Analysis of Monomer–Monomer Interactions in CH_3M Tetramers. The most straightforward approach to understanding the stability of the methylalkalimetal tetramers toward dissociation into the four monomers is directly analyzing the interaction between these monomers in the tetramer. The decomposition of the tetramerization energy, shown in Table S1 in the Supporting Information, reveals that the electrostatic interaction ΔV_{elstat} is the dominant bonding force. This term first decreases from -292.7 (CH_3 –Li) to -205.7 (CH_3Na) and increases thereafter to -209.5 (CH_3K) and further to -240.1 kcal/mol (CH_3Rb). The sudden decrease of ΔV_{elstat} from the methyl lithium to the methylsodium tetramer is partially caused by the relatively large increase in C–M distance if one goes from Li to Na. Furthermore, the trend in ΔV_{elstat} parallels the trend in charge separation as reflected by the alkali metal atomic charges collected in Table 6. According to both the VDD and Hirshfeld method, the metal atomic charge in CH_3M decreases from Li to Na and then increases along Na, K, and Rb. This agrees perfectly with the trend in dipole moment: $\mu = 5.6, 5.2, 6.9,$ and 7.7 D along Li, Na, K, and Rb (see Table 6).

These trends can be understood as resulting from the interplay of two effects. The first one is the increasing extent of charge separation that results as the methyl group moves farther away from the metal atom as the latter becomes larger going from Li to Rb. Thus, the negative charge gained by the methyl group due to the formation of the polar $2a_1 + ns$ electron-pair bond penetrates less into the region of the metal atom and is increasingly associated with the carbon atom. This is schematically depicted by **5a** and **5b**, which represent the situation in a shorter and a longer C–M bond, respectively (the dashed lines represent the bond midplanes):

Table 6. Metal Atomic Charge $Q(M)$ of Methylalkalimetal Oligomers, Carbon Atomic Charge $Q(C)$ in Methyl Fluoride, and Dipole Moment μ^a

	Q(M) in CH ₃ M				Q(M) in (CH ₃ M) ₄				Q(F) in CH ₃ F	
	Li	Na	K	Rb	Li ^b	Na ^b	K ^c	Rb ^c	CH ₃ F	CH ₃ F ^d
VDD (au)	0.386	0.351	0.428	0.466	0.143	0.311	0.343	0.333	-0.142	-0.312
Hirshfeld (au)	0.495	0.417	0.493	0.534	0.306	0.428	0.509	0.527	-0.137	-0.295
μ (D)	5.629 ^e	5.212	6.855	7.723	0	0	0	0	1.808	3.989

^a At BP86/TZ2P. ^b Tetramer with methyl C–H bonds and metal atoms eclipsed. ^c Tetramer with methyl C–H bonds and metal atoms staggered. ^d CH₃F with C–F bond elongated to C–Li distance in CH₃Li (2.010 Å). ^e Agrees well with CCSD(T)/MT(ae) value of 5.643 D, see ref 4b.



The above provides an important insight. It shows that atomic charge values not only depend on the extent of interaction and mixing between fragment orbitals or wave functions but also on the bond distance: the larger the bond distance, the larger the charge separation. This is nicely illustrated by a numerical experiment with methyl fluoride: the fluoride atomic charge in CH₃F amounts to -0.142 and -0.137 au using VDD and Hirshfeld, respectively (see Table 6). This is, in absolute terms, much less than the corresponding lithium atomic charges of +0.386 and +0.495 au in CH₃-Li (see Table 6). However, if we elongate the C–F bond in methyl fluoride from its equilibrium value of 1.395 to 2.010 Å (the length of the C–Li bond in methyllithium), the negative fluoride atomic charge increases significantly, although the SOMO–SOMO mixing across the C–F bond slightly decreases: $Q(F)$ in this deformed CH₃F amounts to -0.312 and -0.295 au using VDD and Hirshfeld (see Table 6). Likewise, the weight of the methyl $2a_1$ SOMO in the C–M bonding $2a_1 + ns$ combination increases only marginally along Li–Rb and cannot be held responsible for the significant changes of the atomic charges along this series.

Superimposed on the above mechanism, which on its own would cause a steady increase of the charge separation (see **5a** and **5b**), there is a second effect, namely the loss (or strong reduction) of the participation of the alkalimetal np_σ AO if one goes from Li to Na because the lithium $2p_\sigma$ AO (-1.3 eV) is at lower energy and therefore a better acceptor orbital than, e.g., the sodium $3p_\sigma$ AO (-0.5 eV) (see Figure 3; orbital energies not shown in figure). This counteracts the former mechanism and causes the alkalimetal atomic charge to decrease from Li to Na. This is because the admixture of the lithium $2p_\sigma$ AO to the electron-pair bonding $2a_1 + 2s$ combination enhances polarization of the charge distribution away from the metal and toward carbon thus increasing the charge separation in CH₃Li, while the effect is absent (or negligible) in CH₃Na. This is schematically illustrated by **6** and **7**, respectively.



The orbital interactions ΔE_{oi} between the CH₃M monomers, although much smaller than ΔV_{elstat} , are still important for the cohesion between the monomers, with values ranging from -82.8 kcal/mol for the methyllithium tetramer to -53.1 kcal/mol for the methylrubidium tetramer (Table S1 in the Supporting Information). Note that these orbital interactions do not involve the formation of an electron-pair bond. They are mainly provided by donor–acceptor interactions between occupied σ_{C-M} and unoccupied σ^*_{C-M} orbitals of the monomers. The net interaction energy ΔE_{int} between CH₃M monomers decreases along M = Li–Rb, steeply at first, from -162.9 to -124.5, and then more gradually to -118.5 and further to -112.8 kcal/mol (see Table S1). The main feature of this trend, that is, the steep decrease in monomer–monomer interaction from methyllithium to the heavier methylalkalimetal systems, is preserved in the overall tetramerization ΔE_{tetra} , which varies from -125.3 for CH₃Li to -73.5, -85.2, and -85.2 for CH₃Na, CH₃K, and CH₃-Rb, respectively.

The analyses of the C–M electron-pair bond in the preceding section also provide insight, in a complementary and maybe a somewhat more indirect fashion, into the stabilizing effect of tetramerization, in particular, the cohesion within the inner alkalimetal cluster in the methylalkalimetal tetramers. In the first place, we have seen that considerable $ns-np$ hybridization (Figure 6) of the alkalimetal relieves the M–M repulsion in the valence state of M_4 , and, in case of Li, it even leads to an overall stabilizing interaction of -6.7 kcal/mol (see $\Delta E_{prep}[M_4]$ in Table 5). The cohesion within M_4 is further enhanced by the interaction with the outer tetrahedron of methyl radicals, especially for Li and Na, because for these metals the M–M bonding qa_1 SOMO of M_4 keeps much of its population, whereas the three M–M antibonding rt_2 SOMOs of M_4 are always more strongly depopulated (see Table 5). This is naturally reflected by the overall energy change $\Delta E_{homo} = \Delta E_{int} + \Delta E_{prep}[(CH_3)_4] + \Delta E_{prep}[M_4]$ for the formation of (CH₃M)₄ from 4CH₃ + 4M (Table 5), the value of which exceeds (i.e., is more stabilizing than) four times the value of ΔE_{homo} for one monomer (Table 4). This excess stabilization is by definition the tetramerization energy ΔE_{tetra} . As we have seen, it decreases indeed steeply if one goes from methyllithium ($\Delta E_{tetra} = -125.3$ kcal/mol) to the heavier congeners ($\Delta E_{tetra} = -73.5$ to -85.2 kcal/mol, see Table S1).

3.6. Polar Bonds and the Concepts of Covalency and Ionicity. Covalency and Ionicity. In the preceding sections, we have established that the C–M bond in methylalkalimetal oligomers has substantial covalent character, especially the C–Li bond in methyllithium, if one considers the sizable

orbital mixing and the fact that the trend in bond strength is dominated by the bond overlap. This is quite at variance with the current picture of this bond being predominantly “ionic”.^{2–4f} Note however that this current view is not based on bond energies and mechanisms but instead on analyses of the charge distribution, using methods such as Streitwieser’s integrated projected population (IPP), Weinhold’s natural population analysis (NPA), and Bader’s atoms in molecules (AIM) approach.²¹ These analyses yield Li atomic charges in methyllithium of +0.8 au with IPP at HF/SS+d,^{2a} +0.85 au with NPA at MP4(SDQ)/6-31+G*,⁵ and +0.90 au with AIM at HF/6-31G**^{4f,1,22} (this agrees well with our AIM value of +0.89 au at BP86/TZ2P).⁹ This led to the idea that the C–Li bond is 80–90% ionic. The problem with quantifying the extent of ionicity on the basis of atomic charges is that different approaches have different scales. The value of the atomic charge of one and the same atom in exactly the same molecule can differ significantly for different methods. The Li atomic charge is, for example, +0.85 au according to NPA,⁵ but according to Hirshfeld¹⁵ and our Voronoi deformation density (VDD) method,¹⁴ it amounts to +0.50 au and +0.39 au, respectively (see Table 6). These values are rather robust regarding the choice of exchange-correlation functional with fluctuations along LDA, BP86, BLYP, OLYP, PW91, and OPBE of 0.03 au for Hirshfeld and only 0.01 au for VDD. Our Hirshfeld and VDD values of +0.50 au and +0.39 au appear to be very close to the GAPT (generalized atomic polar tensors) charge of +0.4178 au computed by Cioslowski at the HF/6-31G** level.^{4k} Again, this does not justify an absolute valuation of 50, 39, or 42% “ionic”. The point is that atomic charges can not simply be interpreted as *absolute* bond polarity indicators.⁹ Atomic charges become meaningful, in principle, only through the comparison of trends computed with one and the same method. In this context, it is an asset of direct-space integration methods such as Hirshfeld and especially VDD that they provide a transparent picture of how the electronic density is redistributed among the atoms due to the formation of chemical bonds. Thus, while Hirshfeld and VDD atomic charges differ somewhat in their absolute values, they both indicate that the charge separation across the C–M bond in methylalkalimetal monomers decreases from Li to Na and increases thereafter along Na, K, and Rb (see Table 6; compare discussion about 5–7 in section 3.5). Both methods indicate also that tetramerization leads to a marked decrease of charge separation for M = Li (compare section 3.4).

It is thus desirable that a definition of the extent of ionicity *I* or covalency *C* involves a definition of both the purely ionic and covalent situation. In the context of MO theory, this can be achieved using the relative contribution *x* of the SOMO of one of the fragments, say the more electronegative one (here: the methyl radical), to the C–M electron-pair bonding MO. The purely ionic situation occurs for $x = x_I = 1$: the unpaired electron of the metal atom is completely transferred to the methyl SOMO which transforms, without admixture of the metal AO, into a lone-pair-like MO in the overall molecule. The purely covalent situation occurs for $x = x_C = 0.5$: the radical electrons of both fragments pair-up

Chart 2

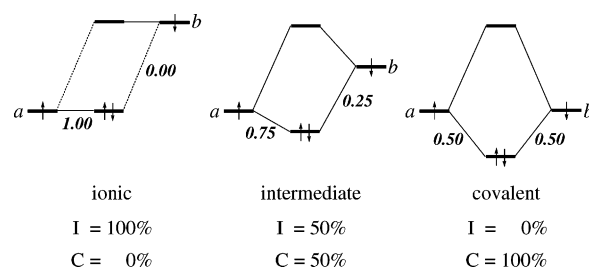


Table 7. Covalency *C* (in %) of Carbon–Metal Bonding in Methyl Alkalimetal Monomers and Tetramers^a

M	CH ₃ M	(CH ₃ M) ₄ ^b A ₁	(CH ₃ M) ₄ ^b T ₂
Li	60 (60)	94 (93)	52 (52)
Na	58 (58)	70 (71)	34 (34)
K	54 (52)	44 (45)	36 (35)
Rb	58 (55)	42 (42)	46 (45)

^a At BP86/TZ2P. *C* is computed with eq 7 using for *x* the Gross Mulliken contribution of the methyl 2a₁ SOMO to the electron-pair bonding combination (see values in Figures 3 and 4). Value in parentheses: idem, using for *x* the Gross Mulliken Population *P* that the methyl 2a₁ SOMO acquires in all occupied MOs of the overall molecule (see values in Tables 4 and 5) divided by 2, i.e., $x = P/2$.
^b Tetramer with methyl C–H bonds and metal atoms eclipsed (Li, Na) or staggered (K, Rb).

in an electron-pair bonding combination of the overall molecule that has equal contributions from either fragment SOMO. The percentage ionicity *I* and covalency *C* is then defined as in eqs 6 and 7, respectively, with $I + C = 100\%$.

$$I = \frac{x - x_C}{x_I - x_C} \times 100\% \quad (6)$$

$$C = \frac{x_I - x}{x_I - x_C} \times 100\% \quad (7)$$

This definition of ionicity and covalency has the advantage of a well-defined scale (i.e., the range of possible values is known), and the interpretation is firmly embedded in the MO model. This is illustrated in Chart 2, which shows the purely ionic and the purely covalent situation as well as a bond of intermediate polarity. We have used this notion of ionicity and covalency already earlier in the discussion in a qualitative fashion. As such, it is in fact widely used throughout MO theory.¹⁸

In Table 7, we have collected percentages of covalency *C* of the C–M bonds of our methylalkalimetal oligomers based on eq 7 using two ways of computing the fraction *x*. In the first one, *x* is the Gross Mulliken contribution of the methyl 2a₁ SOMO to the electron-pair bonding combination in the overall molecule (see values in Figures 3 and 4). Thus, the C–Li electron-pair bond in the methyllithium monomer is 60% covalent and that in A₁ symmetry of the tetramer is even 94% covalent! Covalency is reduced to 52% in the three C–Li electron-pair bonds in T₂ symmetry of the tetramer. The covalent character *C* of the C–M bond decreases from Li to the heavier alkalimetals, slightly so for the monomers, and more pronouncedly for the tetramers (in particular the A₁ component). Also, the difference in *C* between the more covalent A₁ and the more polar T₂ components in the tetramers decreases rapidly along Li–Rb.

There are still other possible ways to compute x , for example, on the basis of the Gross Mulliken population P (see values in Tables 4 and 5) that the methyl $2a_1$ SOMO acquires in all occupied MOs of the overall molecule ($x = P/2$: see values in parentheses in Table 7) or on the basis of fragment MO coefficients (not shown in Table 7). Note that the particular values of C and I depend on how x is computed. One must be aware that this introduces again a certain arbitrariness making C and I semiquantitative rather than quantitative. Nevertheless, any choice for x produces the same trends in C and I , i.e., a nearly constant extent of covalency of the C–M bond going from Li to the heavier alkalimetals, and the occurrence in the tetramer of methyl-lithium and to a lesser extent methylsodium of a more covalent component in A_1 and a more ionic component in T_2 symmetry. The quantities C and I as defined by eqs 6 and 7 also have a more practical disadvantage: they always require the analysis of the orbital electronic structure of the fragments as well as the bonding mechanism in the overall molecule. Thus, computing C and I is much less straightforward than the routine and automated computation of, e.g., VDD or Hirshfeld atomic charges.

Heterolytic Dissociation. So far, we have examined the extent of orbital mixing, its importance for trends in the bond strength and the polarity or charge separation in the C–M bond. Yet another criterion for classifying the C–M bond as covalent is its strong intrinsic preference for dissociating homolytically and not ionically or heterolytically (see section 3.2). To enable a quantitative comparison with other bonds, we have computed the ratio of $\Delta E_{\text{hetero}}/\Delta E_{\text{homo}}$ as a measure for this preference using bond energy values from Table 2. The $\Delta E_{\text{hetero}}/\Delta E_{\text{homo}}$ ratios of CH_3Li – CH_3Rb amount to 3.9, 5.0, 4.9, and 5.0, respectively. Thus, a methyl radical and alkalimetal atom are much closer in energy to the resulting methylalkalimetal molecule than the corresponding ionic fragments. Interestingly, the above $\Delta E_{\text{hetero}}/\Delta E_{\text{homo}}$ ratios of the C–M bonds are higher than the corresponding ratio of the C–H bond in methane which amounts to only 3.8. Apparently, the C–M bond has an even higher relative preference for homolytic dissociation than the slightly polar C–H bond, which is generally taken in organic chemistry as a covalent bond.

Yet, a number of observations has inspired a description of the C–M bond that corresponds to heterolytic or ionic dissociation, namely, in terms of the interaction between a methyl (or, more in general, an organyl) anion and an alkalimetal cation. One of these observations is that, according to IPP, NPA, and AIM, the alkalimetal obtains a large positive charge of 0.8–0.9 au (see, however, above in this section).^{2a,22} Furthermore, it appears that geometries of oligomers and trends in stability can be predicted assuming aggregates consisting of carbanions and metal cations,^{2b,3c,22} although only to some extent.^{3c,4j} And, finally, it is well established that organoalkalimetal compounds react in condensed-phase reactions through ionic mechanisms.¹

The problem with the above is that there is only an indirect relationship between these observations and the extent of polarity of the C–M bond or its preference for either homolytic or ionic dissociation. We have already pointed

Table 8. Analysis of the Carbon–Metal Bond between CH_3^- and M^+ in Methylalkalimetal Monomers^a

	$\text{CH}_3\text{--Li}$	$\text{CH}_3\text{--Na}$	$\text{CH}_3\text{--K}$	$\text{CH}_3\text{--Rb}$
ΔE_{A_1}	–15.2	–16.7	–14.5	–15.7
ΔE_{E_1}	–5.9	–3.8	–3.2	–3.3
ΔE_{oi}	–21.1	–20.5	–17.7	–19.0
ΔE_{Pauli}	44.0	42.5	44.5	55.5
ΔV_{elstat}	–197.4	–178.6	–158.4	–161.9
ΔE_{int}	–174.5	–156.6	–131.6	–125.4
ΔE_{prep}	0.2	0.8	0.6	0.8
ΔE_{hetero}	–174.3	–155.8	–131.0	–124.6

^a Bond energy decomposition (in kcal/mol) at BP86/TZ2P.

out above that the alkalimetal atomic charge is not an absolute bond polarity indicator. Furthermore, the ionic behavior of organoalkalimetal compounds in reactions is inherently a property of the entire reaction system. The latter comprises not only the organoalkalimetal molecule but also all other reactants involved, including the solvent. In general, interactions with solvent molecules promote heterolytic relative to homolytic dissociation because they stabilize situations involving charge separation. Thus, also bonds of which the covalent character is generally accepted, can behave ionically. The C–H bond, for instance, behaves (i.e., dissociates) ionically if a base abstracts a proton from a carbon acid.^{1b} Likewise, nucleophilic substitution is an example of a reaction system in which a (polar) covalent bond (e.g., carbon–halogen or carbon–oxygen) behaves ionically due to the interaction with a nucleophile.^{1b}

Nevertheless, it is instructive to carry out an ionic analysis of the C–M bond, that is, a bond energy decomposition of the interaction between CH_3^- and M^+ in CH_3M (see Table 8) and to compare this with the analysis of the interaction between CH_3^\bullet and M^\bullet in the same molecule (Table 4). In the ionic approach, the classical electrostatic interaction ΔV_{elstat} becomes the dominant bonding term with values that vary from –197.4 to –178.6 to –158.4 to –161.9 kcal/mol along Li–Rb (Table 8). On the other hand, the orbital interaction ΔE_{oi} becomes significantly smaller with values that vary from –21.1 to –20.5 to –17.7 to –19.0 kcal/mol along Li–Rb (Table 8). This has previously been interpreted as suggesting that, compared to the homolytic approach, the charge redistribution in the ionic analysis is smaller, that is, that the ionic fragments correspond more closely to the final charge distribution in the alkalimetal molecule than the neutral methyl and alkalimetal radical fragments.⁵ Another factor, not directly related to the extent of charge redistribution, that may cause the reduced ΔE_{oi} in the ionic analysis is the fact that we lose the stabilization associated with the electron dropping from the SOMO of the metal atom into the C–M bonding MO. The enormous increase in ΔV_{elstat} compared to the homolytic approach (compare Tables 4 and 8) is simply due to the energetically unfavorable charge separation that we enforce by our choice to completely transfer one electron from one of the constituting fragments of CH_3M to the other. It is perfectly valid to carry out such an analysis. Note however that the results refer to the high-energy process of heterolytic bond breaking (eq 5) and *not* to the energetically preferred homolytic bond dissociation (eq 4). Likewise, the ionic C–M interaction ΔE_{int} between

$(\text{CH}_3)_4^{4-}$ and M_4^{4+} in the tetramers $(\text{CH}_3\text{M})_4$ is significantly higher than that between the neutral $(\text{CH}_3)_4$ and M_4 mainly because of the much more stabilizing electrostatic interaction ΔV_{elstat} in the former (compare Tables 5 and S2 in the Supporting Information). The origin is again the energetically highly unfavorable charge separation associated with the complete transfer of four electrons from tetralithium to tetramethyl. The preparation energies $\Delta E_{\text{prep}}[(\text{CH}_3)_4^{4-}]$ and $\Delta E_{\text{prep}}[\text{M}_4^{4+}]$ are highly endothermic mainly because of electrostatic repulsion between the methyl anions and between the alkalimetal cations (see Table S2 in the Supporting Information). Note that the strongly stabilizing electrostatic interaction ΔV_{elstat} between $(\text{CH}_3)_4^{4-}$ and M_4^{4+} compensates for the highly destabilizing preparation energies $\Delta E_{\text{prep}}[(\text{CH}_3)_4^{4-}]$ and $\Delta E_{\text{prep}}[\text{M}_4^{4+}]$. This reflects that the C–M distances in $(\text{CH}_3\text{M})_4$ are shorter than the corresponding C–C and M–M distances (see Table 1).

Comparison with C–X Bond in Methyl Halides. To place our results into a broader chemical context, we have compared the C–M bond in methylalkalimetal monomers CH_3M with the C–X bond in methyl halides CH_3X with X = F, Cl, Br, and I. In a DFT study at BP86 and a basis set similar to ours, Deng et al.²³ found that the trend in C–X bond strength is governed by the difference in electronegativity between CH_3 and X and not by the bond overlap between the methyl $2a_1$ and halogen np_σ SOMOs ($n = 2-5$ along F–I). Thus, the C–X bond strength *decreases* (ref 23a: $\Delta E_{\text{homo}} = -119.4, -87.5, -75.8, -65.2$ kcal/mol) as the halogen atom becomes less electronegative along F–I (this work, Figure 2: $\epsilon(2p_\sigma) = -13.8, -10.1, -9.2, -8.3$ eV), even though the bond overlap increases (ref 23a: $\langle 1a_1 | np_\sigma \rangle = 0.26, 0.34, 0.35, 0.36$). This is highly interesting in the light of our present results. As pointed out earlier, the C–X bond is considered polar covalent and certainly not ionic. Yet, the trend in C–X bond strength of methyl halides along F–I suggests more polar character than the trend in C–M bond strength of methylalkalimetal molecules along Li–K. The explanation is not the absence in methyl halides of covalent features in the bonding mechanism, that is, interaction between and mixing of the methyl and halogen SOMOs.²³ The observed trend is caused instead by the fact that the electronegativity changes much more strongly along the halogen atoms than along the alkalimetal atoms (Figure 2: compare $\epsilon(np_\sigma)$ along F–I with $\epsilon(ns)$ along Li–Rb; see also ref 20a). This agrees well with the fact that the weight of the methyl $2a_1$ SOMO in the bonding $2a_1 + ns$ combination does actually not increase very much along the series (see Figure 3). Therefore, the trend in C–X bond strengths follows the electronegativity of the halogen atoms, whereas the trend in C–M bond strength correlates with the bond overlap.

4. Conclusions

The C–M bond in methylalkalimetal oligomers has substantial covalent character: it can well be viewed as an electron-pair bond between the SOMOs of the methyl radical and alkalimetal atom that gains substantial stabilization from the $\langle 2a_1 | ns \rangle$ bond overlap. This is not in contradiction with this electron-pair bond being highly polar, but it

disqualifies the current classification of the C–M bonding mechanism as “mainly ionic”.

These insights emerge from our quantum-chemical analyses of the methylalkalimetal monomers CH_3M and tetramers $(\text{CH}_3\text{M})_4$ with M = Li, Na, K, and Rb, at BP86/TZ2P. These analyses reveal significant orbital mixing in the C–M electron-pair bond of CH_3M between the methyl $2a_1$ and alkalimetal ns SOMOs (approximately 70% $2a_1 + 25\%$ ns). The C–M bond becomes longer and weaker, both in the monomers and tetramers, if one goes from Li to the larger and more electropositive Rb. Quantitative bonding analyses show that this trend is not only determined by decreasing electrostatic attraction but also, even to a larger extent, by the weakening in orbital interactions. The latter become less stabilizing along Li–Rb because the bond overlap $\langle 2a_1 | ns \rangle$ decreases as the metal ns atomic orbital (AO) becomes larger and more diffuse. Note that for a predominantly ionic bond, one would expect that the orbital interactions are *strengthened* along with the increasing difference in electronegativity between CH_3 and M along Li–Rb. Covalency of the C–M bond is further enhanced in the tetramers, especially for Li and to a lesser extent Na, because in the central M_4 cluster, the alkalimetal becomes effectively less electropositive. The C–M bond has furthermore a slightly stronger intrinsic preference for homolytic dissociation than, for example, the C–H bond, which is generally considered covalent.

Earlier evidence for classifying the C–Li bond as 80–90% ionic based on lithium atomic charges is not conclusive because atomic charges are *no absolute* bond polarity indicators. Different atomic charge methods have different scales and yield evidently different values for the same situation: *only trends* of atomic charges computed with one and the same method can be physically meaningful. Finally, while it is true that the polarity of a bond is the net result of the various features in the bonding mechanism, it is not true that this bonding mechanism and the relative importance of all its features (e.g., electrostatic attraction, bond overlap, charge transfer) can be deduced from the bond polarity in a straightforward manner.

Acknowledgment. Dedicated to Professor Gernot Frenking on the occasion of his 60th birthday. We thank the following organizations for financial support: the HPC-Europa program of the European Union, the Deutsche Akademische Austauschdienst (DAAD), The Netherlands Organization for Scientific Research (NWO), the Ministerio de Educación y Cultura (MEC), the Training and Mobility of Researchers (TMR) program of the European Union, the Dirección General de Enseñanza Superior e Investigación Científica y Técnica (MEC-Spain), and the DURSI (Generalitat de Catalunya). Excellent service by the Stichting Academisch Rekencentrum Amsterdam (SARA) and the Centre de Supercomputació de Catalunya (CESCA) is gratefully acknowledged.

Supporting Information Available: On-scale representation of CH_3M , $(\text{CH}_3\text{M})_4$ ecl, and $(\text{CH}_3\text{M})_4$ stag (M = Li, Rb) and additional analyses of the C–Li bond in CH_3Li_4 and monomer–monomer interactions as well as a

heterolytic approach to C–M bonding in methyl alkalimetal tetramers. This material is available free of charge via the Internet at <http://pubs.acs.org>.

References

- (1) See, for example: (a) Elschenbroich, Ch. *Organometallics*, 3rd ed.; Wiley-VCH: Weinheim: Germany, 2006. (b) March, J. *Advanced Organic Chemistry*, 4th ed.; Wiley-Interscience: New York, 1992.
- (2) (a) Streitwieser, A., Jr.; Williams, J. E., Jr.; Alexandratos, S.; McKelvey, J. M. *J. Am. Chem. Soc.* **1976**, *98*, 4778. (b) Streitwieser, A., Jr. *J. Organomet. Chem.* **1978**, *156*, 1.
- (3) (a) Kremer, T.; Harder, S.; Junge, M.; Schleyer, P. v. R. *Organometallics* **1996**, *15*, 585. (b) El-Nahas, A. M.; Schleyer, P. v. R. *J. Comput. Chem.* **1994**, *15*, 596. (c) Lambert, C.; Schleyer, P. v. R. *Angew. Chem.* **1994**, *106*, 1187; *Angew. Chem., Int. Ed. Engl.* **1994**, *33*, 1129. (d) Lambert, C.; Kaupp, M.; Schleyer, P. v. R. *Organometallics* **1993**, *12*, 853. (e) Kaufmann, E.; Raghavachari, K.; Reed, A. E.; Schleyer, P. v. R. *Organometallics* **1988**, *7*, 1597. (f) Bauer, W.; Winchester, W. R.; Schleyer, P. v. R. *Organometallics* **1987**, *6*, 2371. (g) Haeflner, F.; Brinck, T. *Organometallics* **2001**, *20*, 5134. (h) Gohaud, N.; Begue, D.; Pouchan, C. *Chem. Phys.* **2005**, *310*, 85. (i) Gohaud, N.; Begue, D.; Pouchan, C. *Int. J. Quantum Chem.* **2005**, *104*, 773. (j) Bushby, R. J.; Steel, H. L. *J. Organomet. Chem.* **1987**, *336*, C25. (k) Bushby, R. J.; Steel, H. L. *J. Chem. Soc., Perkin Trans 2* **1990**, 1143.
- (4) (a) Kwon, O.; Sevin, F.; McKee, M. L. *J. Phys. Chem. A* **2001**, *105*, 913. (b) Breidung, J.; Thiel, W. *J. Mol. Struct.* **2001**, *599*, 239. (c) Scalmani, G.; Brédas, J. L. *J. Chem. Phys.* **2000**, *112*, 1178. (d) Fressigné, C.; Maddaluno, J.; Giessner-Prettre, C. *J. Chem. Soc., Perkin. Trans 2* **1999**, 2197. (e) Tyerman, S. C.; Corlett, G. K.; Ellis, A. M.; Claxton, T. A. *J. Mol. Struct. (THEOCHEM)* **1996**, *364*, 107. (f) Wiberg, K.; Breneman, C. M. *J. Am. Chem. Soc.* **1990**, *112*, 8765. (g) Schiffer, H.; Ahlrichs, R. *Chem. Phys. Lett.* **1986**, *124*, 172. (h) Dill, J. D.; Schleyer, P. v. R.; Binckley, J. S.; Pople, J. A. *J. Am. Chem. Soc.* **1977**, *99*, 6159. (i) Graham, G. D.; Marynick, D. S.; Lipscomb, W. N. *J. Am. Chem. Soc.* **1980**, *102*, 4572. (j) Sapse, A. M.; Raghavachari, K.; Schleyer, P. v. R.; Kaufmann, E. *J. Am. Chem. Soc.* **1985**, *107*, 6483. (k) Cioslowski, J. *J. Am. Chem. Soc.* **1989**, *111*, 8333. (l) Ponec, R.; Roithová, J.; Gironés, X.; Lain, L.; Torre, A.; Bochicchio, R. *J. Phys. Chem. A* **2002**, *106*, 1019.
- (5) Bickelhaupt, F. M.; van Eikema Hommes, N. J. R.; Fonseca Guerra, C.; Baerends, E. J. *Organometallics* **1996**, *15*, 2923.
- (6) Experimental structures of methyl alkalimetal monomers: (a) Grotjahn, D. B.; Pesch, T. C.; Brewster, M. A.; Ziurys, L. M. *J. Am. Chem. Soc.* **2000**, *122*, 4735. (b) Grotjahn, D. B.; Apponi, A. J.; Brewster, M. A.; Xin, J.; Ziurys, L. M. *Angew. Chem., Int. Ed. Engl.* **1998**, *37*, 2678. (c) Grotjahn, D. B.; Pesch, T. C.; Xin, J.; Ziurys, L. M. *J. Am. Chem. Soc.* **1997**, *119*, 12368. (d) Andrews, L. *J. Chem. Phys.* **1967**, *47*, 4834.
- (7) Experimental structures of methyl alkalimetal tetramers: (a) Weiss, E.; Lambertsen, T.; Schubert, B.; Cockcroft, J. K.; Wiedenmann, A. *Chem. Ber.* **1990**, *123*, 79. (b) Weiss, E.; Corbelin, S.; Cockcroft, J. K.; Fitch, A. N. *Angew. Chem.* **1990**, *102*, 728; *Angew. Chem., Int. Ed. Engl.* **1990**, *29*, 650. (c) Weiss, E.; Corbelin, S.; Cockcroft, J. K.; Fitch, A. N. *Chem. Ber.* **1990**, *123*, 1629. (d) Weiss, E.; Lambertsen, T.; Schubert, B.; Cockcroft, J. K. *J. Organomet. Chem.* **1988**, *358*, 1. (e) Weiss, E.; Hencken, G. *J. Organomet. Chem.* **1970**, *21*, 265.
- (8) (a) Günther, H.; Moskau, D.; Bast, P.; Schmalz, D. *Angew. Chem., Int. Ed. Engl.* **1987**, *26*, 1212. (b) Bauer, W.; Schleyer, P. v. R. *Adv. Carbanion Chem.* **1992**, *1*, 89. (c) Bauer, W. *Lithium Chemistry*; Wiley-Interscience: New York, 1995. (d) Fraenkel, G.; Martin, K. V. *J. Am. Chem. Soc.* **1995**, *117*, 10336. (e) Ebel, H. F. *Tetrahedron* **1965**, *21*, 699. (f) Armstrong, D. R.; Perkins, P. G. *Coord. Chem. Rev.* **1981**, *38*, 139.
- (9) Fonseca Guerra, C.; Handgraaf, J.-W.; Baerends, E. J.; Bickelhaupt, F. M. *J. Comput. Chem.* **2004**, *25*, 189.
- (10) Bickelhaupt, F. M.; Baerends, E. J. In *Rev. Comput. Chem.*; Lipkowitz, K. B., Boyd, D. B., Eds.; Wiley-VCH: New York, 2000; Vol. 15, pp 1–86.
- (11) (a) te Velde, G.; Bickelhaupt, F. M.; Baerends, E. J.; van Gisbergen, S. J. A.; Fonseca Guerra, C.; Snijders, J. G.; Ziegler, T. *J. Comput. Chem.* **2001**, *22*, 931. (b) Fonseca Guerra, C.; Snijders, J. G.; te Velde, G.; Baerends, E. J. *Theor. Chem. Acc.* **1998**, *99*, 391. (c) Fonseca Guerra, C.; Visser, O.; Snijders, J. G.; te Velde, G.; Baerends, E. J. In *Methods and Techniques for Computational Chemistry*; Clementi, E., Corongiu, G., Eds.; STEF: Cagliari, 1995; pp 305–395. (d) Baerends, E. J.; Ellis, D. E.; Ros, P. *Chem. Phys.* **1973**, *2*, 41. (e) Boerrigter, P. M.; te Velde, G.; Baerends, E. J. *Int. J. Quantum Chem.* **1988**, *33*, 87. (f) te Velde, G.; Baerends, E. J. *J. Comput. Phys.* **1992**, *99*, 84. (g) Snijders, J. G.; Baerends, E. J.; Vernooijs, P. *At. Nucl. Data Tables* **1982**, *26*, 483. (h) Krijn, J.; Baerends, E. J. *Fit Functions in the HFS Method; Internal Report* (in Dutch); Vrije Universiteit: Amsterdam, 1984. (i) Slater, J. C. *Quantum Theory of Molecules and Solids Vol. 4*; McGraw-Hill: New York, 1974. (j) Vosko, S. H.; Wilk, L.; Nusair, M. *Can. J. Phys.* **1980**, *58*, 1200. (k) Becke, A. D. *J. Chem. Phys.* **1986**, *84*, 4524. (l) Becke, A. *Phys. Rev. A* **1988**, *38*, 3098. (m) Perdew, J. P. *Phys. Rev. B* **1986**, *33*, 8822 (Erratum: *Phys. Rev. B* **1986**, *34*, 7406). (n) Fan, L.; Ziegler, T. *J. Chem. Phys.* **1991**, *94*, 6057.
- (12) Atkins, P. W. *Physical Chemistry*; Oxford University Press: Oxford, 1982.
- (13) (a) Morokuma, K. *J. Chem. Phys.* **1971**, *55*, 1236. (b) Kitaura, K.; Morokuma, K. *Int. J. Quantum Chem.* **1976**, *10*, 325. (c) Bickelhaupt, F. M.; Nibbering, N. M. M.; van Wezenbeek, E. M.; Baerends, E. J. *J. Phys. Chem.* **1992**, *96*, 4864. (d) Ziegler, T.; Rauk, A. *Inorg. Chem.* **1979**, *18*, 1558. (e) Ziegler, T.; Rauk, A. *Theor. Chim. Acta* **1977**, *46*, 1.
- (14) The Voronoi deformation density (VDD) method was introduced in ref 5. See also: (a) ref 9. (b) Fonseca Guerra, C.; Bickelhaupt, F. M.; Snijders, J. G.; Baerends, E. J. *Chem. Eur. J.* **1999**, *5*, 3581. Voronoi cells are equivalent to Wigner-Seitz cells in crystals; for the latter, see: (c) Kittel, C. *Introduction to Solid State Physics*; Wiley: New York, 1986.
- (15) Hirshfeld, F. L. *Theor. Chim. Acta* **1977**, *44*, 129.
- (16) Note that, for a proper comparison, we have to remove the zero-point vibrational energy (ΔZPE) correction (obtained at the HF level) that is contained in the UB3LYP bond energies of ref 3a using our own BP86 ΔZPE corrections, which yields UB3LYP values for ΔE_{homo} of -45.7 , -31.1 , -27.2 , and -24.6 kcal/mol along $M = \text{Li, Na, K, and Rb}$.
- (17) The description of the MO in terms of fragment MO coefficients instead of Gross Mulliken contributions yields the same picture, but it has the disadvantage of not being normalized, that is, the figures do not add up to 1 (or to 100%). Note that diffuse fragment MOs (often at higher energy) can make unphysical negative Gross Mulliken contributions, which are then compensated by positive Gross

Mulliken contributions that exceed 100%. This problem occurs in a slight form also in our systems in which the sum of the main positive Gross Mulliken contributions to the C–M electron-pair bonding combination are in some cases 101%–103% (M = Li and Na in Figures 3 and 4).

- (18) (a) Albright, T. A.; Burdett, J. K.; Whangbo, M.-H. *Orbital Interactions in Chemistry*; Wiley-Interscience: New York, 1985. (b) Gimarc, B. M. *Molecular Structure and Bonding – The Qualitative Molecular Orbital Approach*; Academic Press: New York, 1979.
- (19) The C–M bond distance also increases along Li–Rb because of the increasing number of metal core shells that enter into Pauli repulsion with closed shells on the methyl fragment. For a discussion on how the interplay of bonding and repulsive orbital interactions determines bond lengths, see, for example: Bickelhaupt, F. M.; DeKock, R. L.; Baerends, E. J. *J. Am. Chem. Soc.* **2002**, *124*, 1500.
- (20) (a) Mann, J. B.; Meek, T. L.; Allen, L. C. *J. Am. Chem. Soc.* **2000**, *122*, 2780. (b) Allen, L. C. In *Encyclopedia of Computational Chemistry*; Schleyer, P. v. R., Ed.; Wiley: New York, 1998; Vol. 2.
- (21) (a) Collins, J. B.; Streitwieser, A., Jr.; McKelvey, J. M. *J. Comput. Chem.* **1979**, *3*, 79. (b) Reed, A. E.; Curtiss, L. A.; Weinhold, F. *Chem. Rev.* **1988**, *88*, 899. (c) Bader, R. W. F. *Atoms in Molecules, A Quantum Theory*; Clarendon Press: Oxford, U.K., 1990.
- (22) Wiberg, K. B.; Rablen, P. R. *J. Comput. Chem.* **1993**, *14*, 1504.
- (23) (a) Deng, L.; Branchadell, V.; Ziegler, T. *J. Am. Chem. Soc.* **1994**, *116*, 10645. For a related study, see: (b) Bickelhaupt, F. M.; Ziegler, T.; Schleyer, P. v. R. *Organometallics* **1996**, *15*, 1477.

CT050333S